

by

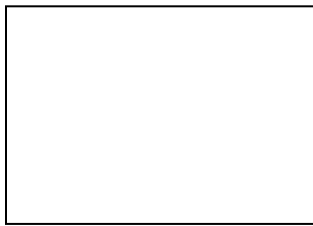
**Dr. Ed Marotta, Dr. L.S. Fletcher, Thermal Conduction Laboratory
Department of Mechanical Engineering
Texas A&M University**

Project Report – Phase One

**Prepared for the Minerals Management Service
Under the MMS/OTRC Cooperative Research Agreement
1435-01-04-CA-35515
Task Order 35663
Project Number 509**

December 2005

OTRC Library Number: 12/05A160



For more information contact:

Offshore Technology Research Center

Texas A&M University
1200 Mariner Drive
College Station, Texas 77845-3400
(979) 845-6000

or

Offshore Technology Research Center

The University of Texas at Austin
1 University Station C3700
Austin, Texas 78712-0318
(512) 471-6989

A National Science Foundation Graduated Engineering Research Center

Interstitially Insulated Coaxial Pipe

By

Dr. Ed Marotta
Dr. L.S. Fletcher
Thermal Conduction Laboratory
Department of Mechanical Engineering
Texas A&M University

ABSTRACT

The increasing demand for oil is causing exploration to reach into greater ocean depths. The ocean floor temperature increases the risk of the crude oil cooling to a temperature that could result in flow blockage from paraffin formation. Oil companies could potentially spend millions correcting this problem due to lost production time. In order to mitigate this problem, appropriate insulation is added to the pipe to maintain the oil at its extraction temperature, and thus, help minimize paraffin formation. This project investigates how an interstitially insulated coaxial pipe with a metal wire mesh can provide improved insulation properties with simplified pipe construction and production issues. By increasing the thermal resistance within the sub-sea pipe, the thermal energy leaving the oil and entering the cold sub-sea environment is decreased.

Experiments have been conducted to determine the heat transfer conductance coefficient for this proposed interstitially insulated coaxial pipe technology and the results have been compared to existing insulation techniques. Different interstitial materials have been tested, including Stainless Steel, Titanium, Inconel, and Tungsten. Along with varying the wire material, the mesh number was varied, determining its effect on the overall thermal joint conductance. Moreover, a Mylar film was added to the test matrix as an additional layer of insulation/resistance. It was determined that a 5 mesh stainless steel wire screen with a Mylar film inserted at the interface between the two layers of pipe material provided the best insulation characteristics. The thermal conductance of the air/wire screen composite was experimentally measured as low as $42.0 \text{ W/m}^2\text{-K}$ ($7.40 \text{ Btu/ft}^2 \text{ hr } ^\circ\text{F}$), which translates to an effective thermal conductivity of 0.08 W/m-K ($0.05 \text{ Btu/ft hr } ^\circ\text{F}$), at an interface pressure of 172.3 kPa (25.0 psi). These values compare very favorably with current insulation technologies whose effective thermal conductivity range from 0.12 to 0.15 W/m-K (0.07 to $0.09 \text{ Btu/ft hr } ^\circ\text{F}$).

Thus, a comparison of the interstitially insulated coaxial pipe with current technologies has shown the interstitially insulated coaxial pipe to be a potential means to reducing paraffin deposit blockage in deep water pipe-lines and risers. Moreover, the results seem to indicate superior insulating characteristics when compared to current available technologies which have far greater manufacturing complexities. The proposed technology also shows promise for liquefied petroleum gas pipeline/transfer line applications.

TABLE OF CONTENTS

ABSTRACT	<i>ii</i>
NOMENCLATURE	<i>iv</i>
INTRODUCTION	<i>1</i>
<i>Project Background and Motivation</i>	<i>1</i>
ANALYSIS	<i>6</i>
<i>Pipe Resistance</i>	<i>6</i>
<i>Thermal Contact Resistance</i>	<i>10</i>
<i>Wire Mesh Types and Configurations</i>	<i>13</i>
<i>Mesh Size</i>	<i>13</i>
<i>Important Definitions</i>	<i>14</i>
<i>Alternatives to Wire Screen Mesh</i>	<i>14</i>
<i>Mesh Selection Criteria</i>	<i>15</i>
<i>Mesh Material Selection</i>	<i>15</i>
<i>Design Factors to Consider</i>	<i>16</i>
EXPERIMENTAL INVESTIGATION	<i>20</i>
<i>Purpose</i>	<i>20</i>
<i>Test Plan #1</i>	<i>26</i>
<i>Test Plan #2</i>	<i>21</i>
<i>Machine Cylinder Inserts</i>	<i>21</i>
<i>Apparatus Design Overview</i>	<i>28</i>
<i>Data Acquisition System</i>	<i>26</i>
<i>Data Analysis</i>	<i>26</i>
<i>Experimental Procedure</i>	<i>26</i>
<i>Data Acquisition</i>	<i>26</i>
RESULTS AND DISCUSSIONS	<i>29</i>
CONCLUSIONS	<i>35</i>
REFERENCES	<i>36</i>
APPENDIX A- THERMAL EXPERIMENTAL DATA	<i>38</i>
APPENDIX B- UNCERTAINTY	<i>43</i>
APPENDIX C- WIRE SCREEN LITERATURE	<i>55</i>
APPENDIX D - CONVERSION CHART	<i>61</i>

NOMENCLATURE

A_i	=	inner tube cross-sectional area, apparent interface area (m^2)
A_c	=	cross-sectional area (m^2)
h_j	=	joint conductance ($W/m^2 K$)
k	=	thermal conductivity ($W/m K$)
L	=	tube length – tubular pipe analysis set to unity (m)
m	=	semi major axis parameter (m)
P	=	contact pressure (Pa or Psi)
R	=	thermal resistance (K/W)
R_c	=	thermal contact resistance (K/W)
r_i	=	inner pipe radius (m)
r_1	=	outer pipe radius and inner radius of Mylar [®] (m)
r_2	=	outer radius of Mylar [®] and inner radius of the wire screen (m)
r_3	=	outer radius of wire screen and inner radius of Mylar [®] (m)
r_4	=	outer radius of Mylar [®] and inner radius of second pipe (m)
r_5	=	outer radius of second pipe (m)
T	=	surface temperature (K)
t	=	insulation or wire screen mesh thickness (m)
\dot{Q}	=	heat transfer rate (W)
U	=	Overall Heat Transfer Coefficient ($W/m^2 K$)
Δ	=	geometric physical parameter
ΔT_i	=	temperature drop between the two interfaces (K)
Ψ	=	geometric constriction parameter (Dimensionless)
α	=	wire spacing parameter (m)

INTRODUCTION

Project Background and Motivation

As the world continues to rely on the internal combustion engine as its major transportation source, the demand for oil will continue to increase. The exceedingly high demand for crude oil has led industry leaders to pursue offshore exploration in even deeper water, seeking new oil reservoirs. The deeper the oil exploration, the more critical the technology needed to ensure consistent oil flow and equipment maintenance. The valves, manifolds and other flow-line equipment used to transport the oil are operated at ocean floor temperatures that range from 0°C to 2°C (32°F to 35°F).

Crude oil generally contains a type of wax that contains long, straight paraffin chains which stay dissolved when maintained at production temperatures. If the crude oil is exposed to temperatures below the paraffin cloud point, approximately 68°C (155°F), the wax will begin to crystallize into solid particles and deposit on the interior surface of the pipeline. Figure 1 is an example of excessive paraffin build-up, which can lead to complete pipeline blockage.

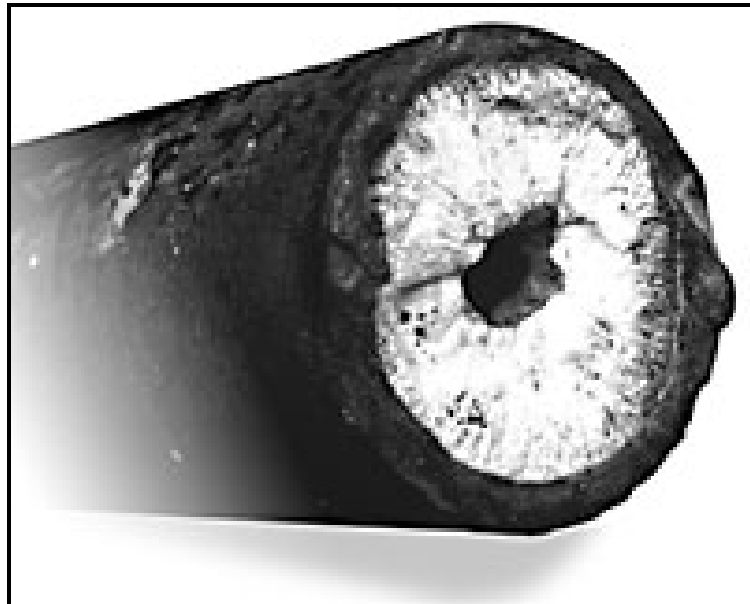


Fig. 1: Waxy Build Up Inside a Pipe Line^[1]

The average ocean floor temperature is approximately 0°C to 2°C (32°F to 35°F), almost freezing. The oil production temperatures are above 70°C (159°F) and this temperature difference is very difficult to maintain. Current insulation solutions for pipelines, such as coated pipe, pipe-in-pipe, and syntactic foam, have limitations in thermal conductivity, hydrostatic pressure, and installation techniques ^[1,2,3]. As a consequence, it is important to explore alternative insulation techniques which will improve the thermal performance of deepwater pipelines.

The current techniques for minimizing the formation of paraffin on interior pipeline walls include pipe-in-pipe heat exchanger concepts, exterior thermal insulation, and external heating sources, as well as oil additives or chemicals. Pipe-in-pipe heat exchangers rely on a thermal resistance network of convection and conduction to prevent heat transfer from the hot oil. Thermal insulation and external heating sources also function to maintain high product temperatures, whereas chemical additives endeavor to lower the cloud temperature of the paraffin in the oil. Pigging, on the other hand, is a process of removing the paraffin build-up on the interior wall, as shown in Figure 2.

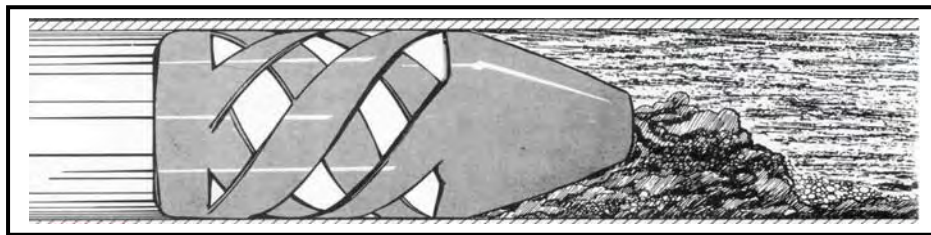
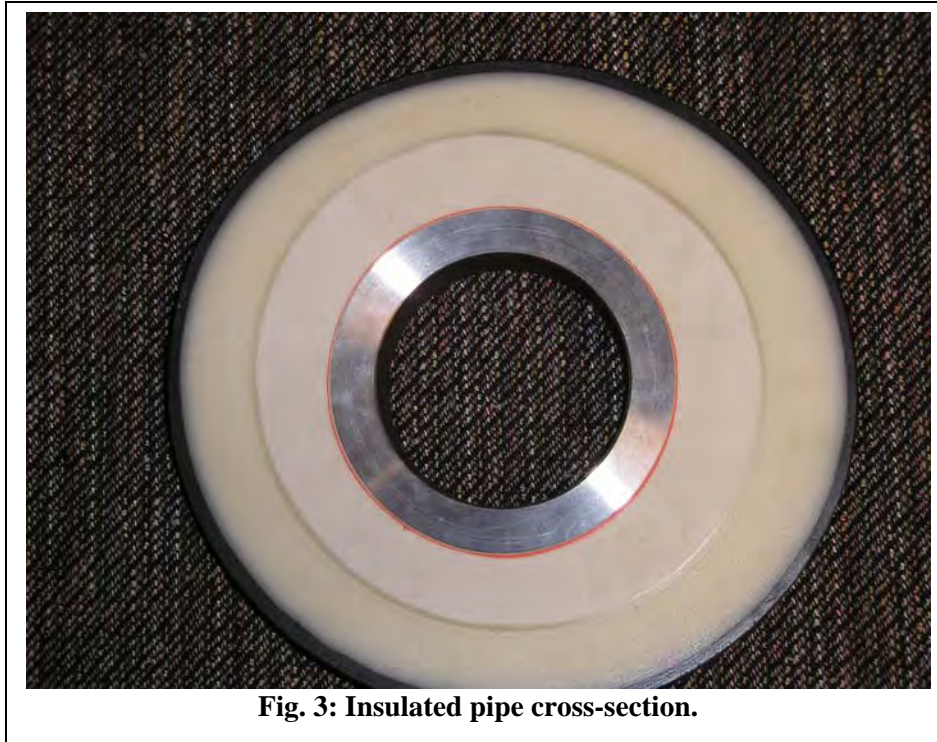


Fig. 2: Pig Running Through a Clogged Pipe ^[1]

Thermal insulation added to the exterior of the pipeline, the technique most commonly used in the Gulf of Mexico, is used to maintain the temperature of the production oil above the cloud temperature for paraffin. A typical example of an insulated deepwater pipeline is shown in the cross-section of an insulated pipe, Figure 3.



This project investigates the benefit of coaxial pipe with a low conductivity screen mesh added between the inner and outer pipe. The screen mesh serves as a means of increasing the thermal resistance of the pipe wall. Such an interstitially insulated pipeline will decrease the thermal loss of the flowing oil, delay the onset of paraffin crystallization, and delay or prevent the deposit of paraffin on the interior wall of the pipe, depending upon the length of the pipeline. In turn, the need to “pig” the pipeline may be delayed or eliminated.

The proposed Interstitially Insulated Coaxial Pipe configuration consists of a wire mesh with or without aluminized Mylar[®] film on either side. The purpose for this configuration, shown in Fig.4, is to reduce the heat transfer rate by allowing for the collection of air pockets, within the wire screen layer at a precise gap thickness, beyond the present commercially available technologies. Thermal resistance is created by the separation of the two surfaces, or interface, via the wire screen. The addition of Mylar[®] layers, a strong polyester film, to the inner lining of the pipe provides further insulation and heat resistance. Ultimately, the thermal resistance impedes the flow of heat energy, thus preventing the paraffin in the oil from reaching its cloud point.

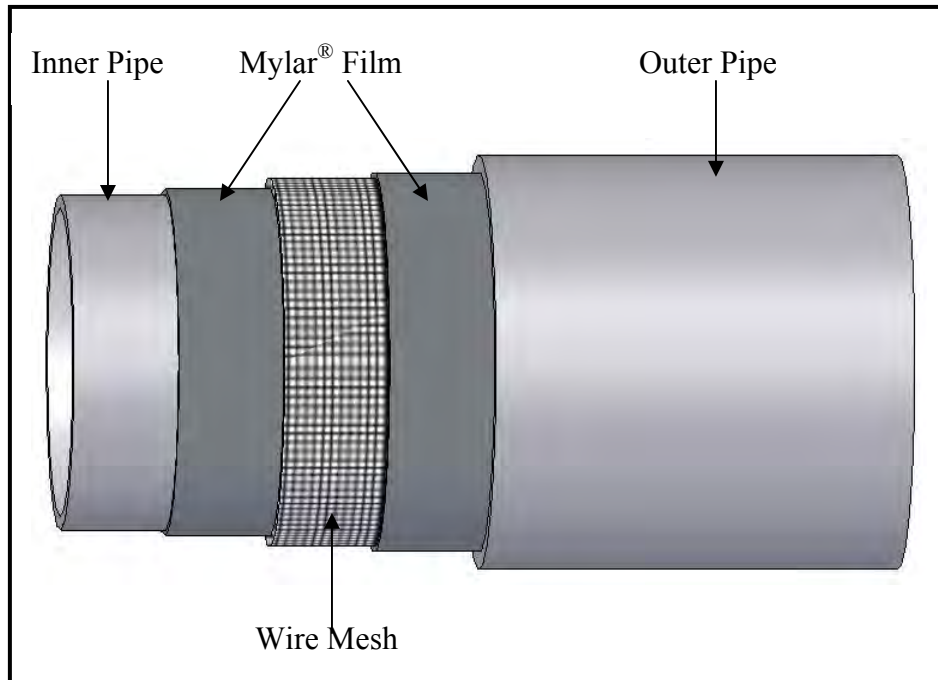


Fig. 4: Interstitially Insulated Coaxial Pipe (IICP) Configuration.

This report describes the analytical modeling and experimental investigation conducted to determine the potential benefits of the Interstitially Insulated Pipe. The results of a number of experimental tests are presented and recommendations are made as to the most appropriate design for such pipe.

The report is divided into the following sections: 1) Analysis – analytical expressions are developed and used to aid in the prediction and comparison of thermal resistance performance against a current commercially available technology. This effort involves the addition of the thermal resistance due to the air gap and the thermal resistance due to the contact resistance caused by the wire screen inserted between concentric layers of a tubular pipe, 2) Experimental Investigation – an experimental study was undertaken to ascertain the level of thermal resistance achievable with the wire screen technology. This section details the test plan executed which includes such physical, mechanical, and thermophysical properties which lead to the reduction in the heat transfer rate across the air gap separated by the wire screen, 3) Results and Discussion – the experimental data are shown as the thermal joint conductance as a function of the applied interface pressure for three simulated temperatures that range between the elevated oil temperature and the cold seawater temperature. Moreover, the experimental results compare the

measured thermal joint conductance against contact configurations which include smooth contacting surfaces, highly roughened contacting surfaces, and 4) Conclusion – a summary of the main findings and observations as a result of this study are presented.

ANALYSIS

Thermal resistance has been defined as a resistance to heat conduction⁴. An analogous electrical circuit can be used in lieu of differential equations in the calculation of the heat transfer rate. Figure 5 explains the analogy for the resistances between electrical flow and thermal transport.

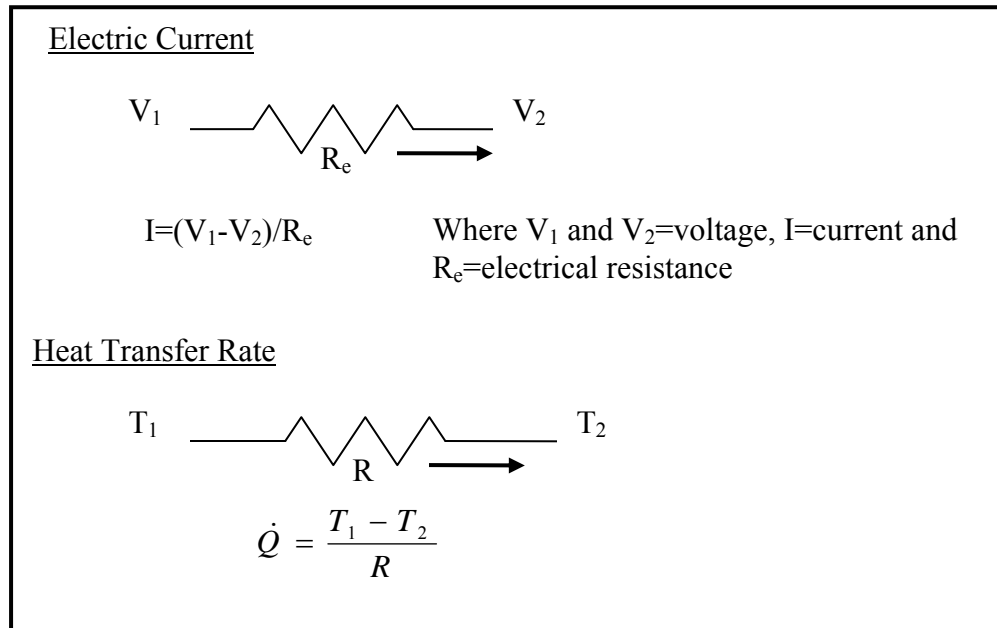


Fig. 5: Analogy between Electric Current and Heat Transfer Rate

To define a standard for comparison, the overall heat transfer coefficient of a pipe covered with insulation and polypropylene can be defined by summing the thermal resistances of each layer. The development of these equations for the pipe with standard present-day insulation, and then with a wire screen inserted at its center are developed.

Pipe Resistance

A heat transfer analysis for a cylindrical pipe can be modeled using criteria for multilayered cylinders^[4]. For simplification purposes, the pipe is modeled as a circular cross-section by unit length and focusing the heat loss only in the radial direction. Since the overall heat transfer coefficient of the pipe is needed, the thermal resistance is the key variable that must be found first. Finding the overall heat transfer coefficient of the pipe without the wire mesh first will

allow us to compare the heat transfer characteristics to the pipe with the screen mesh. Figure 6 illustrates this view without the screen mesh with labeled radii.

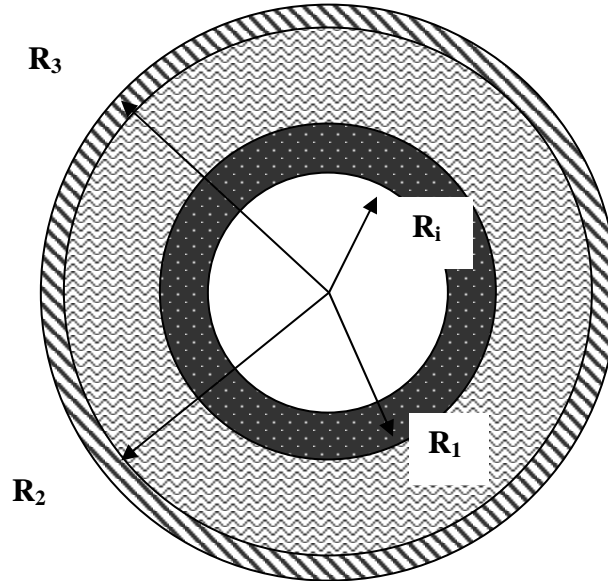


Fig. 6: Cross-section of pipe without wire screen.

The inner radius of the pipe is labeled R_i , and the outer radius of the pipe is labeled R_1 , which also corresponds to the inner radius of the insulation. The outer layer of the insulation is labeled R_2 , which also corresponds to the inner layer of the polypropylene exterior coating, and the outer layer of the whole pipe is R_3 . From this figure equations can be developed using fundamentals of heat transfer. These equations are based on heat conduction in multilayered cylinders and spheres. Eq. 1, gives the overall thermal contact resistance of the pipe without the screen mesh.

$$R_{tot} = R_{pipe} + R_{insulation} + R_{polypropylene} \quad \left(\frac{K}{W} \right) \quad (1)$$

The next set of equations will define the individual equations of the contact resistance for the pipe, insulation, and polypropylene.

$$R_{pipe} = \frac{\ln\left(\frac{r_1}{r_i}\right)}{2\pi k_{pipe} L} \quad \left(\frac{K}{W}\right) \quad (2)$$

$$R_{insulation} = \frac{\ln\left(\frac{r_2}{r_1}\right)}{2\pi k_{insulation} L} \quad \left(\frac{K}{W}\right) \quad (3)$$

$$R_{polypropylene} = \frac{\ln\left(\frac{r_3}{r_2}\right)}{2\pi k_{polypropylene} L} \quad \left(\frac{K}{W}\right) \quad (4)$$

After all these variables are defined, the Overall Heat Transfer Coefficient, U , per inner cross-sectional area of the tube is found using Eq. 5.

$$U = [A_i R_{tot}]^{-1} \quad \left(\frac{W}{m^2 K}\right) \quad (5)$$

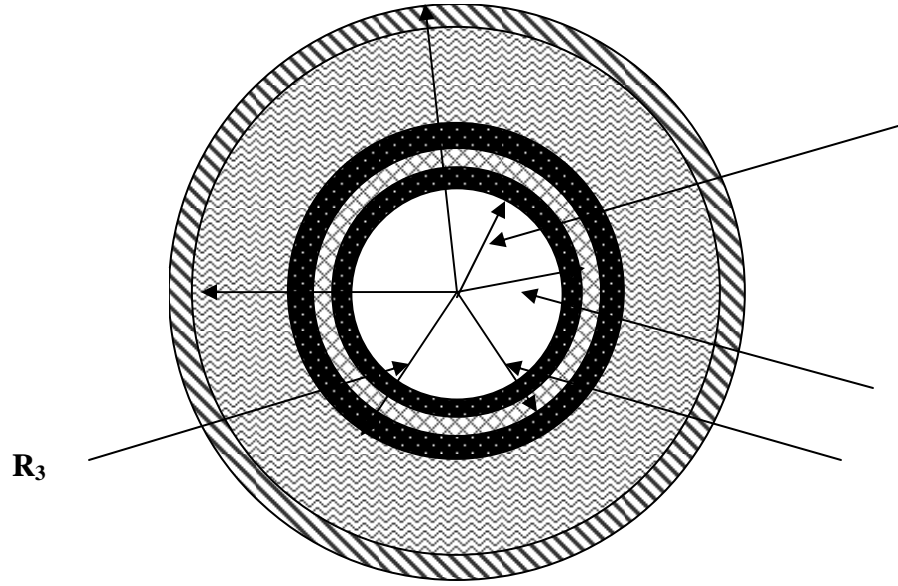
Now that the overall heat transfer coefficient of the pipe without the mesh is known, the coefficient of the pipe with the mesh can now be determined. Figure 7 shows a cross-section view of the pipe with the interstitial wire mesh.

The labeled radii are as follows: pipe inner radius, R_i ; wire mesh inner radius, R_1 ; wire mesh outer radius, R_2 ; pipe outer radius or insulation inner radius, R_3 ; polypropylene coating inner radius or outer radius of insulation, R_4 ; and polypropylene coating outer radius, R_5 . With the wire mesh inserted, it creates added resistance to the pipe insulation, which is the basis of this proposal. The total thermal resistance per unit length of tube is found using Eq. 6.

$$R_{tot} = R_{p,1} + R_{mesh} + R_{p,2} + R_{insulation} + R_{polypropylene} \quad \left(\frac{K}{W}\right) \quad (6)$$

The next set of equations defines the individual resistances of the materials.

$$R_{p,1} = \frac{\ln\left(\frac{r_1}{r_i}\right)}{2\pi k_{p,1} L} \quad \left(\frac{K}{W}\right) \quad (7)$$



$$R_{mesh,1} = \frac{\ln\left(\frac{r_2}{r_1}\right)}{2\pi k_{mesh} L} \quad \left(\frac{K}{W}\right) \quad (8)$$

Equation 8 is what the present research project focuses on. If the value of the wire mesh's thermal conductivity can be as small as possible, the indirect relationship will cause the contact resistance to increase hindering the heat transfer, obtaining the goal of insulating the pipe.

$$R_{p,1} = \frac{\ln\left(\frac{r_3}{r_2}\right)}{2\pi k_{p,2} L} \quad \left(\frac{K}{W}\right) \quad (9)$$

$$R_{insulation} = \frac{\ln\left(\frac{r_4}{r_3}\right)}{2\pi k_{insulation} L} \quad \left(\frac{K}{W}\right) \quad (10)$$

$$R_{polypropylene} = \frac{\ln\left(\frac{r_5}{r_4}\right)}{2\pi k_{polypropylene} L} \quad \left(\frac{K}{W}\right) \quad (11)$$

The overall heat coefficient per inner cross-sectional area of the tube can then be computed using Eq. 6 substituted into Eq.5. Therefore, once the conductance of the wire mesh is determined, by experimentation, the comparison can be drawn and the wire mesh's effectiveness determined [1]. A result of this preliminary calculation is shown in Fig. 8 where values for the wire screen are approximated (horizontal axis), and the affect on the overall pipe resistance can be gleaned.

This analysis enables the setting of targets for the reduction in thermal performance to advance design/thermal technology needed to ensure flow assurance for not only deep-sea applications, but for other oil product applications, liquid natural gas (LNG) transfer, and environmental applications where costs are of particular concern.

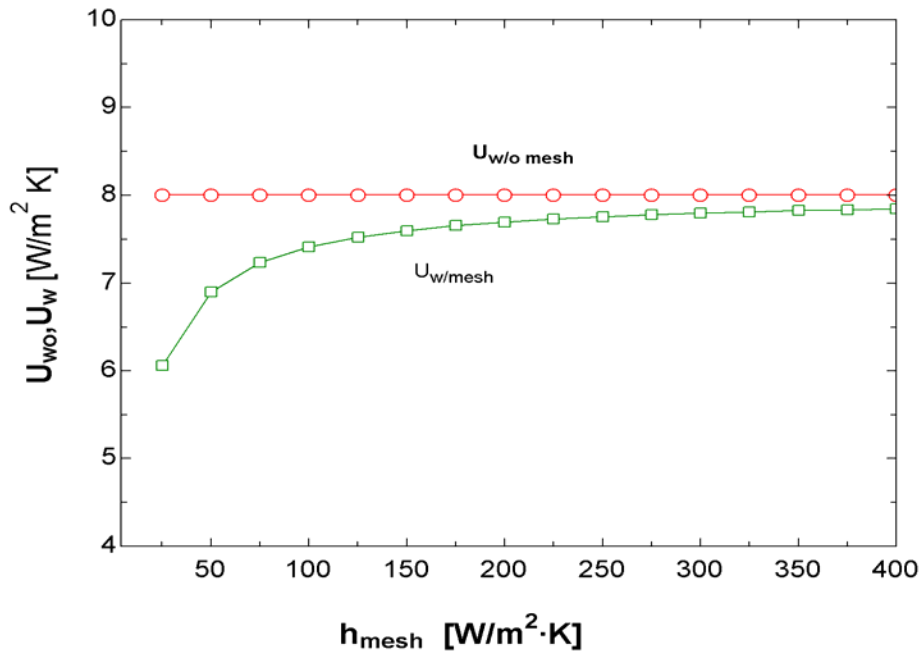


Fig. 8: Analysis of the Overall Thermal Conductance, U , as a function of the thermal conductance of a wire screen placed within a tubular pipe with present day insulation included.

Thermal Contact Resistance

In order to model the geometric aspects of the interface between the flux meter surfaces and the wire mesh, equations were developed, via Cividino et al.⁵, for the thermal constriction resistance due to an isothermal elliptic contact area supplying heat to a half-space. First of all, we define the interface as the joint, which consists of both the wire mesh and two flat metal

surfaces. We assume that interaction between the flat surface and the wire mesh forms an elliptic contact area. Also, when there is interaction between the wires, it forms a circular contact area. Equation (12) gives the expression for the thermal constriction resistance in a flat metal substrate:

$$R_{e1} = \frac{\psi_{e1}^T}{4k_1 m \left[(3/4) P \alpha^2 D^2 \Delta_{12} \right]^{1/3}} \quad \left(\frac{K}{W} \right) \quad (12)$$

Next we assume that the constriction within the wire is equivalent to the resistance within a half-space. This yields the thermal constriction resistance in the wire mesh Eq. (13).

$$R_{e2} = \frac{\psi_{e2}^T}{4k_2 m \left[(3/4) P \alpha^2 D^2 \Delta_{12} \right]^{1/3}} \quad \left(\frac{K}{W} \right) \quad (13)$$

Since both geometric constriction parameters are equal, the total constriction resistance due to one elliptic contact is the sum of Eqs. (12) and (13):

$$R_{e12} = \frac{(2/\pi) K(\kappa) [A+B]^{1/3}}{4k_{12} m \left[(3/4) P \alpha^2 D^2 \Delta_{12} \right]^{1/3}} \quad \left(\frac{K}{W} \right) \quad (14)$$

Since there are two elliptic contact areas, Eq. (15) gives the total constriction resistance for a second elliptic contact.

$$R_{e23} = \frac{(2/\pi) K(\kappa) [A+B]^{1/3}}{4k_{23} m \left[(3/4) P \alpha^2 D^2 \Delta_{23} \right]^{1/3}} \quad \left(\frac{K}{W} \right) \quad (15)$$

Once these are known, the total thermal resistance from substrate 1 to substrate 3 can be determined using Eq. (16).

$$R_{13} = R_{12} + R_{23} \quad \left(\frac{K}{W} \right) \quad (16)$$

The next set of equations gives various parameters needed to calculate the above resistances. Equation (17) is a ratio of the wire spacing and the wire diameter, while Eq. (18) represents a semi major axis parameter.

$$\alpha = \frac{c}{D} \quad (17)$$

$$m = 0.830\alpha^{0.735} \quad (18)$$

Equation (19) is a geometric parameter related to elasticity theory to determine the shape of contact areas.

$$A + B = \frac{1}{D} \left[\frac{\alpha^2 + 3}{\alpha^2 + 1} \right] \quad (19)$$

Equations (20) and (21) define the geometric-physical parameters between their respective substrates.

$$\Delta_{12} = \frac{\left[(1-\nu_1^2)/E_1 \right] + \left[(1-\nu_2^2)/E_2 \right]}{A + B} \quad (20)$$

$$\Delta_{23} = \frac{\left[(1-\nu_2^2)/E_2 \right] + \left[(1-\nu_3^2)/E_3 \right]}{A + B} \quad (21)$$

Equations (22) and (23) give the harmonic mean thermal conductivity of the contact between their respective substrates.

$$k_{12} = \frac{2k_1k_2}{k_1 + k_2} \quad \left(\frac{W}{m \cdot K} \right) \quad (22)$$

$$k_{23} = \frac{2k_2k_3}{k_2 + k_3} \quad \left(\frac{W}{m \cdot K} \right) \quad (23)$$

In summary, the combination of the thermal contact resistance caused by the contact points of the wire mesh and the air gap resistance will affect the overall thermal joint resistance of this technology. The placement of any additional insulating materials to the outer circumference of the tubular pipe will further affect the insulating characteristics of the pipe. The expressions shown will allow the modeling of these effects so that an optimized design can be achieved that needs the functional requirements of not only the pipe, but also, the insulating technology.

The Interstitially Insulated Coaxial Pipe is a new technology which requires investigatory experimentation and analytical modeling in order to find the best possible design. The experimental parameters consist of:

- Mesh size
- Interface temperature
- Contact pressure
- Surface roughness
- Additional layers (Mylar[®])

A survey of wire screen types and configurations is presented of available technologies and materials that can be employed for the Interstitially Insulated Coaxial Pipe technology proposed here.

Wire Mesh Types and Configurations

Several types and configurations of wire mesh screens exist, which are used for various applications. Examples of select mesh configuration and type are shown in Fig.9.

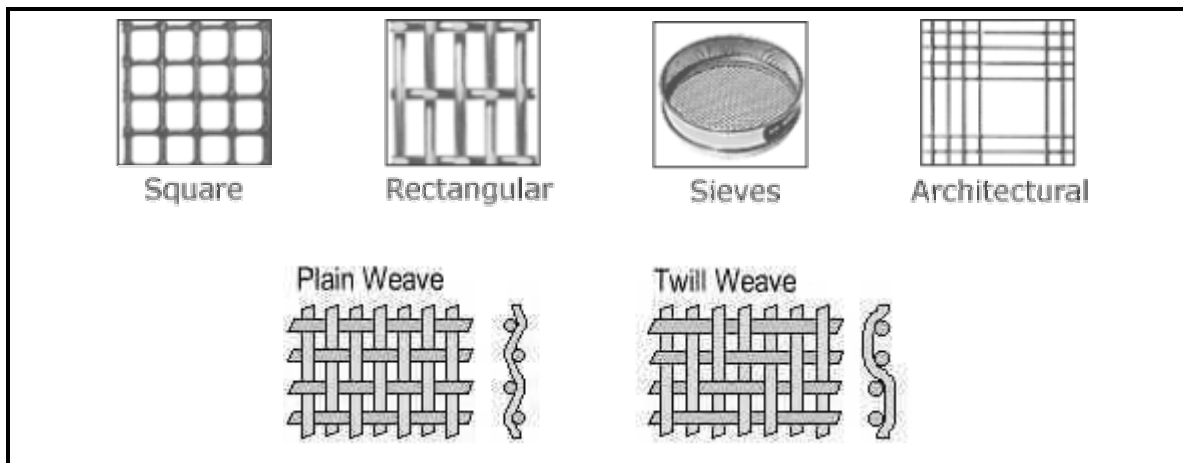


Fig. 9: Collection of Mesh Type and Configuration⁶

Mesh Size

The best way to describe a particular mesh is to identify the type of metal or alloy, spacing between the wires, weave pattern and thickness of wire diameter. For example, the proper mesh call out for a stainless steel mesh with a wire thickness of 1.2mm (0.047 in.) would be: stainless steel gauze, size 4, wire spacing 5.15 mm (0.203 in.)

Important Definitions

Mesh Size: the number of openings from the center of any one wire to the center of a parallel wire one lineal inch away (9). Figure 10 shows a size 2 mesh.

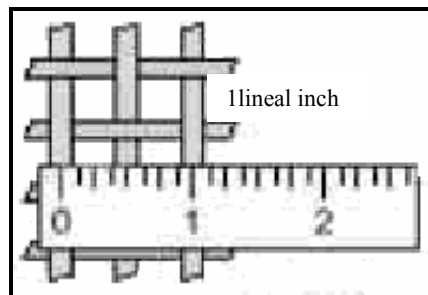


Fig. 10: Definition of Mesh Number⁴

Open Area: the total area of the holes divided by the area of the cloth and is expressed as a percentage. The expressions used to compute these parameters are illustrated in Fig.11 for a square mesh.

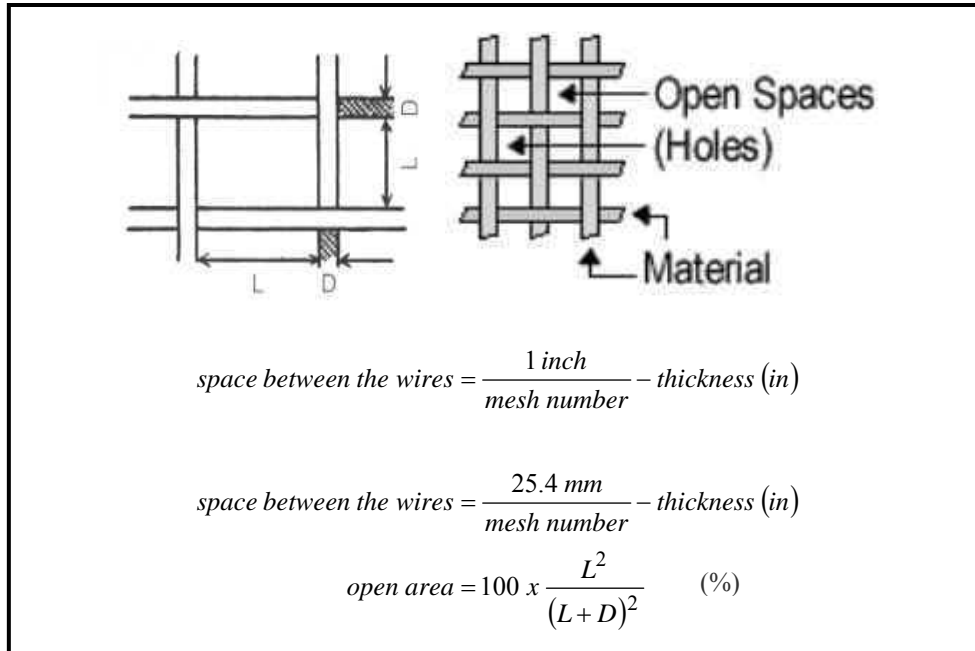
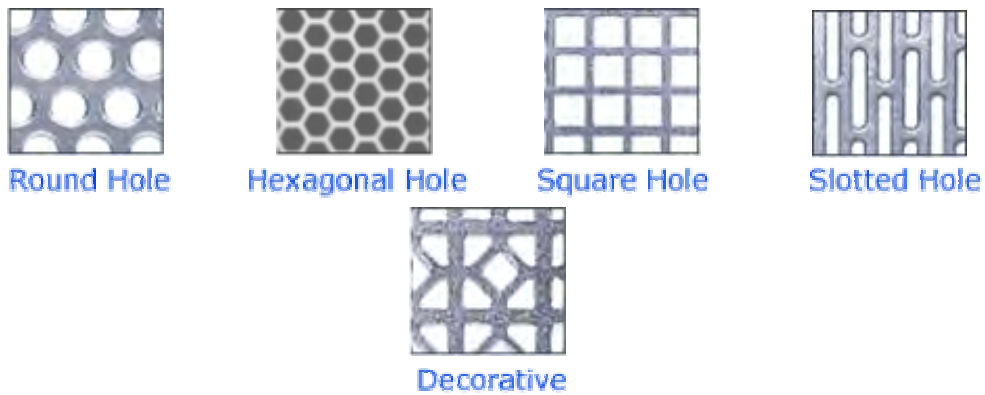


Fig. 11: Calculation of Spaces between Wires and Percent of Open Space⁴
Alternatives to Wire Screen Mesh

Other types of non-weaved wire screen configurations as shown in Fig. 12 can be investigated, but for ease of manufacturability and to maximize the thermal contact resistance, only traditional wire screen configurations were included in this experimental study:

Perforated Metal



Expanded Metal



Fig. 12: Examples of alternative to the conventional wire mesh

Mesh Selection Criteria

As a set of selection criteria, the following factors may be considered along with knowledge of the working environment, when choosing a suitable material for wire screen fabrication:

1. Mesh Geometry^{1, 2}
2. Material service temperatures
3. Material maximum temperatures
4. Manufacturability
5. Corrosion resistance.

Mesh Material Selection

Various materials were researched as possible candidate materials for the wire screen. Various candidate materials which are suitable as a wire screen material and would maximize strength and minimize thermal conduction are shown in Table 1. However, these metals are not necessarily available as a wire screen product, but because of their mechanical properties would make them ideal for our technology application. Both mechanical and thermal material properties, shown in Table 1, of the candidate materials were compared to stainless steel, shown in Table 2. High pressure and temperature exposure require the candidate material to have exceptional mechanical properties, comparable to stainless steel, but lower thermal conductivity. In order to generate higher thermal resistance the thermal properties of any candidate material must significantly supplant that of stainless steel.

A significant limitation on the selection of alternative wire screen material other than stainless steel had to do with manufacturability. Several Inconel alloys were an attractive choice for testing because of their good ductility and ability to be formed with conventional techniques. Table 3 shows the mechanical and thermal properties for several different Inconel and Incoloyl alloys. The compositional break-down for these alloys is shown in Table 4.

Design Factors to Consider

As a set of selection criterions, for a particular application, the following factors must be considered with knowledge of the working environment when choosing a suitable material for wire screen fabrication:

¹ Geometry criteria include open area, mesh type, weight, weld points and wire cross section.

² See appendix for the results of geometric mesh selections

- Material service temperatures
- Material maximum temperatures
- Manufacturability (i.e., mesh size)
- Corrosion resistance.
- Feasibility in the manufacturing of such materials into a size 5 mesh.

The thermal conductivity values, k , values for Titanium, Uranium, Constantan, Inconel, Monel, and Nickel Chromium were estimated using a relation from [4].

Figure 13 shows a cross-sectional view of the pipe setup with the wire mesh inserted. This project quantifies the thermal performance (e.g., thermal joint resistance/conductance) for the portion which encompasses the two contacting surfaces and the wire screen mesh. In addition, this investigation quantifies the joint conductance from the simulated hot oil surface to the simulated cold-seawater Temperature.

Several tests with various materials have provided the overall thermal joint resistance of the wire screen mesh technology. However, the thermal contact resistance is unknown at this point since all testing has been conducted with air present at the gap.

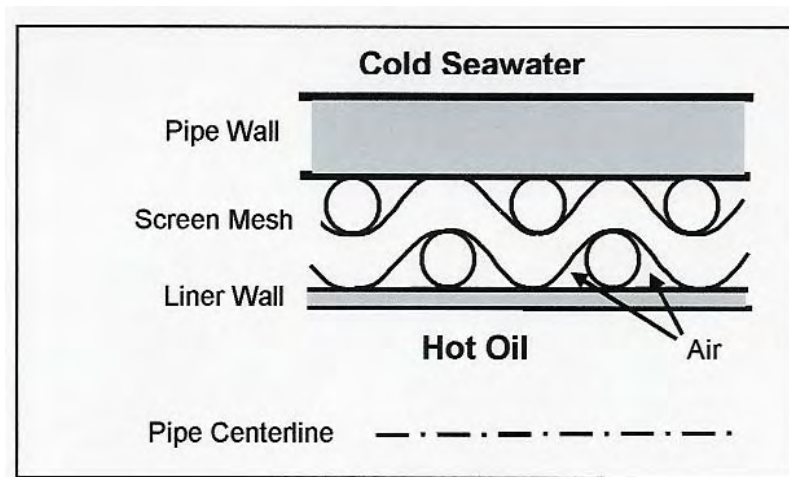


Fig. 13: Cross-section view of pipe insulation with wire mesh³.

Thermal contact resistance modeling will enable the determination of the magnitude for this resistance, and then the combination of the gap resistance in parallel with the contact resistance

³ Marotta, Ed. "Interstitially Insulated Coaxial Pipe." Summary Plan 2004-2005 OTRC Project. 04 June 2004.

can be used to optimize the technology for the greatest overall joint resistance. The analysis for the pipe insulation resistance and the determination of the thermal contact resistance follows. The pipe insulation resistance network is shown because it is employed in a performance comparison with and without the wire screen present in a commercially available insulation configuration.

Table 1: Mechanical and Thermal Properties of Various Metals ⁵

Metal or Alloy	Hardness (Brinell)	Modulus of Elasticity (GPa)	Poisson's Ratio	Melting Point (C)	Thermal Conductivity (W/m-K)
Titanium	70	116	0.34	1650-1670	17
Yttrium	40	63.5	0.243	1515-1531	14.6
Zirconium	145	94.5	0.34	1852	16.7
Tellurium	25	40	0.33	449.5	3.38
Terbium	38 (Vickers)	55.7	0.26	1356-1364	11.1
Samarium	38 (Vickers)	49.7	0.274	1067-1077	13.3
Scandium	132 or 36 (Vickers)	74.4	0.279	1539	6.3
Plutonium	242	96.5	0.15-0.21	640	8.4
Praseodymium	20 (Vickers)	37.3	0.281	927-935	11.7
Neodymium	18 (Vickers)	41.4	0.281	1010	13
Bismuth	7	31.7	0.33	271.3	10
Erbium	42 (Vickers)	69.9	0.237	1522	9.6
Europium	17 (Vickers)	18.2	0.152	817-827	13.9
Gadolinium	37 (Vickers)	54.8	0.259	1310-1312	8.8
Holmium	46 (Vickers)	64.8	0.231	1470	16.2

Table 2: Stainless Steel Comparative Land Mark ^{4, 6}

Stainless Steel	Density (g/cm³)	Elastic Modulus (GPa)	Specific Heat (20 °C) (J/(Kg*K)	Hardness	Thermal Conductivity (20 °C) W/(m*K)
18-S	8.03	190	500	145-160 HB	18

⁴ Table 2 expressed in English units can be found in the Appendix D

Table 3: Mechanical and Thermal Properties for Inconel and Incoloyl Alloys^{6,7}

Alloy	UNS no.	Density (g/cm ³)	Elastic Modulus (GPa)	Specific Heat (20 C) (J/(Kg*K))	Hardness ⁵	Thermal Conductivity (20C) (W/(m*K)) ⁶
Inconel Alloy 600	N0660	8.47	207	444	36 HRC	14.9
Inconel Alloy 625	N06625	8.44	207	410	190 HB	9.8
Inconel Alloy 718	N07718	8.19	211	450	45 HRC	11.4
Inconel Alloy X-750	N07750	8.25	207	431	330 HB	12
Inconel Alloy MA 754	N07754	8.3	160	440	25 HRC	14.3
Incoloyl Alloy 825	N08825	8.14	206	440	75 HRB	11.1
Incoloyl Alloy 909	N19909	8.3	159	427	38 HRC	14.8

Table 4: Elemental Break Down of Inconel and Incoloyl Alloys⁶

Alloy	UNS no.	Nickel	Copper	Iron	Chromium	Molybdenum	Aluminum	Silicon	Magnesium	Carbon	Cobalt	Niobium	Titanium	Yttrium Oxide
Inconel Alloy 600	N0660	75.5	0.5	8	15.5	~	~	0.2	0.5	0.08	~	~	~	~
Inconel Alloy 625	N06625	62	~	2.5	22	9	0.2	0.2	0.2	0.05	~	3.5	0.2	~
Inconel Alloy 718	N07718	52.5	~	18.5	19	3	0.5	0.2	0.2	0.04	~	5	0.9	~
Inconel Alloy X-750	N07750	71	0.5	7	15.5	~	0.7	0.5	1	0.08	~	~	2.5	~
Inconel Alloy MA 754	N07754	78.5	~	~	20	~	0.3	~	~	0.05	1	~	0.5	0.6
Incoloyl Alloy 825	N08825	42	2.2	30	21	3	0.1	0.25	0.5	0.03	~	~	0.9	~
Incoloyl Alloy 909	N19909	38	~	42	~	~	~	0.4	~	0.1	13	4.7	1.5	~

⁵ HB= hardness Brinell, HRC= hardness Rockwell using a brale indenter and a major load of 150kg, HRB=hardness Rockwell using a 1/16 inch ball indenter and a major load of 100kg

⁶ The k values for Titanium, Uranium, Constantan, Inconel, Monel and Nickel Cromium were estimated using a relation from [6].

EXPERIMENTAL INVESTIGATION

The experimental set-up used in conducting these experiments provided a replication of the actual use of the mesh screen. Wire meshes were ordered from several companies with various configuration and material parameters. The type of wire mesh materials which were ordered included 316 stainless steel, titanium, tungsten, and Inconel. Each wire mesh was characterized by its mesh number which represents the wire spacing per linear inch as described in the introduction section. Diameters for each mesh number can be varied as well, but due to manufacturing constraints the mesh numbers that were ordered came with a standard wire diameter for the mesh number.

The same grade of sub-sea pipe steel was ordered to represent actual pipe wall. Pipe steel is characterized by its yield stress, thus in our case, the pipe steel that was ordered was “X-60 or X-80” pipe. Actually, it was determined that this trade-name referred to the yield strength of the pipe. Thus the equivalent grade of steel used for this experimental study to represent pipe steel was medium-carbon steel P110 4140. A test plan was developed to incorporate the main design parameters needed for a successful configuration, which then can be translated over to concept space where functional requirements and performance criteria can be identified and validated through experimentation.

Purpose

The purpose of the first set of experiments was to quantify the thermal performance of Interstitial Insulated Coaxial Pipe. The experimental facility is appropriate for simulating deep-water applications. The thermal joint resistance was measured with circular, 2.54 cm (1 in.), cut outs of stainless steel, titanium, tungsten, and Inconel mesh pressed between two stainless steel slugs (flux meters). A second set of experiments was conducted to collect data pertaining to the effects of surface finish on the thermal joint resistance. The details of the experimental procedure and experimental plans are described below.

In each test run, 4140 pipe steel (P110) was fabricated into 3.81 cm (1.5 in.) long flux meters. Five equally spaced holes were drilled to the center in order to affix “T” type thermocouples as shown by Fig. 14. These thermocouples were used to measure the axial temperature distributions during testing.

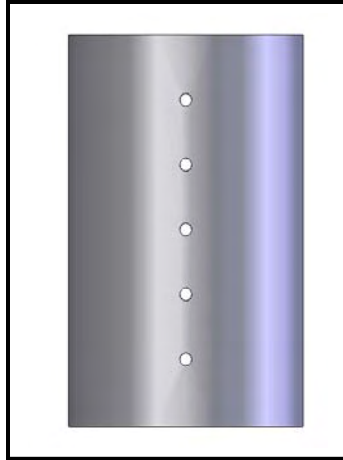


Fig. 14: Pipe Steel P110 4140 Flux Meter

Test Plan - #1

Table 5 summarizes the experiment parameters which were to ascertain the overall thermal joint conductance resulting from the insertion of a wire screen between two separated surfaces with air as the interstitial medium. All wire screens were placed between two Pipe Steel P110 fluxmeters so that the only thermal performance measured was of the wire mesh itself and the adjacent P110 Surfaces.

The experimental study encompassed the range of pressures and temperatures that are typically experienced by sub-sea pipe lines during normal operations. The set of wire mesh materials were chosen because of their high mechanical strength and thermophysical properties, which are suitable for this technology application.

Test Plan - #2

Machine Cylinder Inserts

Steel 4140 bar stock was machined into 1 inch diameter cylinders as shown by Fig. 15. The purpose of the inserts was to simulate the inner and outer piping of the Interstitial Insulating Coaxial Pipe. One cylinder insert would be in contact with the heated flux meter and the other would be in contact with the cooled flux meter. The wire mesh was sandwiched between the two cylinder inserts, thus mimicking the actual Interstitially Insulated Coaxial Pipe technology under actual temperature and pressure conditions of a sub sea environment.

Table 5: Phase (1) Experimental Variable⁷

Mesh Material	Mesh Number	Wire Diameter (cm)	Interface Pressure (kPa)	Outer Temp (C)	Inner Temp (C)	Mean Interface Temp (C)
Stainless Steel	5	0.10414	172.4, 344.7, 517.1, 689.5, 1034.2, 1379, 1723.7, 2068.4, 2758, 3447.4	0	93.3	16.7, 46.7, 86.7
Stainless Steel	10	0.0635	172.4, 344.7, 517.1, 689.5, 1034.2, 1379, 1723.7, 2068.4, 2758, 3447.4	0	93.3	16.7, 46.7, 86.7
Stainless Steel	24	0.03556	172.4, 344.7, 517.1, 689.5, 1034.2, 1379, 1723.7, 2068.4, 2758, 3447.4	0	93.3	16.7, 46.7, 86.7
Titanium	9	0.08128	172.4, 344.7, 517.1, 689.5, 1034.2, 1379, 1723.7, 2068.4, 2758, 3447.4	0	93.3	16.7, 46.7, 86.7
Titanium	14	0.04064	172.4, 344.7, 517.1, 689.5, 1034.2, 1379, 1723.7, 2068.4, 2758, 3447.4	0	93.3	16.7, 46.7, 86.7
Titanium	18	0.02794	172.4, 344.7, 517.1, 689.5, 1034.2, 1379, 1723.7, 2068.4, 2758, 3447.4	0	93.3	16.7, 46.7, 86.7
Tungsten	8	0.0254	172.4, 344.7, 517.1, 689.5, 1034.2, 1379, 1723.7, 2068.4, 2758, 3447.4	0	93.3	16.7, 46.7, 86.7
Tungsten	20	0.0127	172.4, 344.7, 517.1, 689.5, 1034.2, 1379, 1723.7, 2068.4, 2758, 3447.4	0	93.3	16.7, 46.7, 86.7

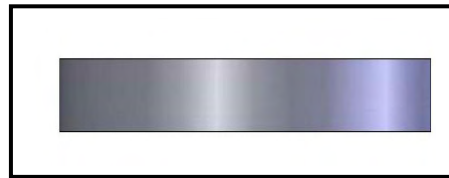


Fig. 15: Cylinder Inserts

Initially the joint contact resistance of two cylinder inserts was measured with just one contacting interface to obtain a reference value for comparison with the Interstitial Insulating Coaxial Pipe technology and a solid pipe wall; this schematic is shown by Fig. 16.

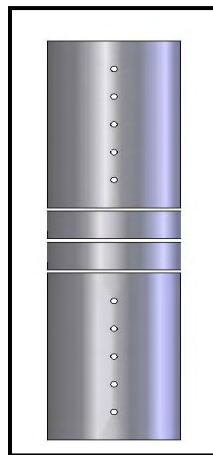


Fig. 16: Cylinder inserts between two flux meters

⁷ Table 5 in English units can be found in the appendix

The next step was to place a wire screen between the two P110 4140 inserts for further comparison of thermal performance as shown by Fig. 17. The results from this scenario were used to evaluate a new wire screen candidate material. An Inconel 625 wire screen was placed between the two cylindrical inserts which were also roughened as well. The joint resistance between the two cylinders at three temperatures and ten pressures were measured similar to Test #1. Table 6 summarizes the experiment variables employed in Test Plan #2.

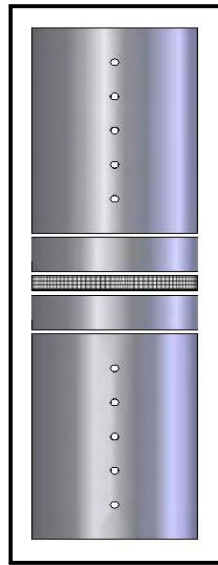


Fig. 17: Flux meters, cylinder inserts wire mesh

In summary, the results from all experimental runs have been plotted as thermal joint resistance/conductance as a function of applied interface pressure at three different interface temperatures (see the Results and Discussion section). The tests attempted to simulated several possible design configurations which would minimize the thermal transfer across the joint, and thus maximize the thermal insulation property of the Interstitially Insulating Coaxial Pipe.

Table 6: Phase (2) Experimental Variables⁸

Surface Finish	Interface Pressure (kPa)	Interface Temperature (K)
Machine finish (not polished)	172.4, 344.7, 517.1, 689.5, 1034.2, 1379, 1723.7, 2068.4, 2758, 3447.4	290
Machine finish (not polished)	172.4, 344.7, 517.1, 689.5, 1034.2, 1379, 1723.7, 2068.4, 2758, 3447.4	320
Machine finish (not polished)	172.4, 344.7, 517.1, 689.5, 1034.2, 1379, 1723.7, 2068.4, 2758, 3447.4	360
Roughened interface surface With Inconel	172.4, 344.7, 517.1, 689.5, 1034.2, 1379, 1723.7, 2068.4, 2758, 3447.4	290
Roughened interface surface With Inconel	172.4, 344.7, 517.1, 689.5, 1034.2, 1379, 1723.7, 2068.4, 2758, 3447.4	320
Roughened interface surface With Inconel	172.4, 344.7, 517.1, 689.5, 1034.2, 1379, 1723.7, 2068.4, 2758, 3447.4	360

Apparatus Design Overview

The Thermal Contact Conductance (TCC) system as shown in Fig. 18 consists of a heat source, three specimens, a heat sink, a load cell and bellows. The apparatus is intended to handle specimens 1 inch in diameter. The bell jar's contents can be entirely evacuated if needed, thus minimizing convection heat transfer at the contact interface and all other surfaces – thus minimizing convective losses; however, these experiments were run with an ambient environment within the bell jar, and therefore, air was present between the gap formed by the contacting surface/wire screen joint.

The gap between the surfaces minimizes the convective heat transfer, and but allows for conductive heat transfer to occur; therefore, the present assembly takes advantage of the low thermal conductivity of air.

⁸ Table 6 expressed in English units can be found in Appendix D

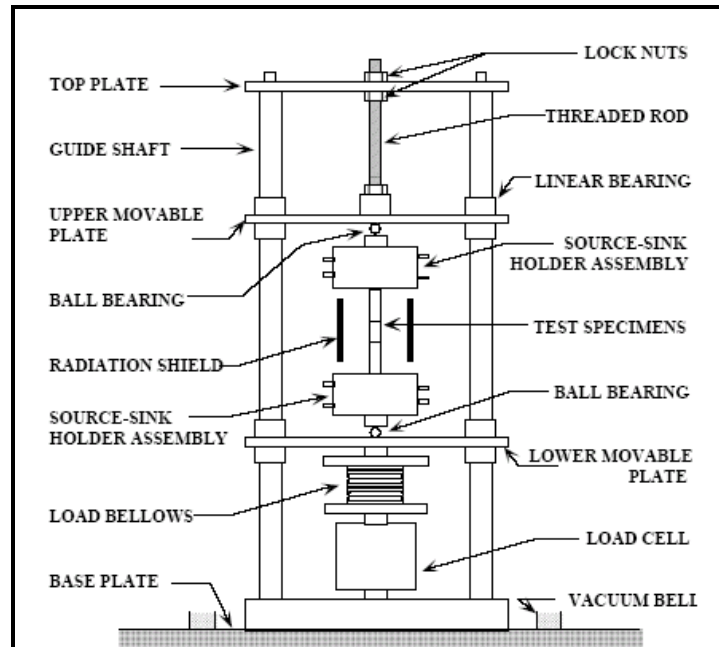


Fig. 18: Apparatus without Hood

The heater was attached to the upper plate and affixed to the heat source at the top of the column. The heat sink was fastened at the bottom of the column and fed with coolant. The refrigerated bath, with a temperature range of -20°C (-4°F) to 150°C (302°F), was controlled by a thermo regulator. To optimize heat transfer coolant was used on all contacting surfaces experiencing heat flow. Radiation shields were placed around the test column to minimized radial heat loss. The shield was located approximately 2.54 cm (1 in.) from the heat source surface and 1.27 cm (0.5 in.) from the specimen.

The test column was loaded by introducing pressure into the stainless steel bellows, mounted at the bottom of the column, using a pressure regulator. A 22,241 N (5000 lb_f) load cell was used to determine the pressure at the interface. Five “T” type thermocouples were affixed to the centerline of each flux meter by packing them tightly into holes using powdered metal. The test column may be operated in a vacuum environment to eliminate the effects of interstitial fluids on the heat transfer at the interface. The roughing pump works in series with an oil diffusion pump to maintain the vacuum at a low level.

Data Acquisition System

The Hewlett Packard 3497A (HP 3497A) Data Logger was used for data acquisition. Depending on the parameter the data acquisition measurements were divided into five categories: voltage, temperature, resistance, frequency and pressure. The system uses a transducer in the form of thermocouples to connect to the system in order to sample system temperatures. The transducer converts the system physical parameter inputs into electrical signals (voltage) which can be measured by the logger via the interface bus. Measurements and data are then transferred and processed for storage and display.

Data Analysis

Once steady state conditions were reached, the data acquisition system is executed. The program utilizes temperature and pressure data, as well as, other information, to calculate the flux through each test column by applying Fourier's Law. The contact conductance, h , is computed using the average heat flux across the test interface divided by the cross sectional area of the test interface divided by the change in temperature across the interface.

Experimental Procedure

The experimental test runs were carefully conducted with a specific procedure developed to accomplish this task; the exact procedure is outlined below on a step by step basis:

All contacting surfaces were thoroughly cleaned, including the wire mesh, with methanol followed by an acetone wash. This is done to remove surface oxides and other organic contaminants. Thermal grease was applied to the contacting surfaces of the bottom and upper flux-meters, and then mounted into the vertical stack/column. In addition, thermal grease was applied to the lower and upper surfaces of the cylinders and mounted within the column.

The wire screen was placed into the column, and then a very low interface pressure was applied to the column such that wire screen plastic deformation did not occur, approximately 89 N (20 lbf) or 172 kPa (25 psi); this was performed to ensure that the column remains as aligned as possible while the pressure is applied while the experimental runs were conducted.

The entire stack/column was wrapped by a secured foam insulation cover which helps to minimize convective losses, and thus ensure that the applied heat flow is one dimensional along

the column. To further reduce convective losses a bell jar was lowered onto an aluminum base and the entire stack was engulfed. At this point the control software program was initiated.

The control system adjusts the temperature and pressure until the test conditions are met. When nominal steady state conditions are reached, up to thirty iterations are performed until the thermal contact conductance value falls within the tolerance range. Data is then collected for all temperature and pressures prescribed. This procedure was followed for all wire screens and other experimental runs for this study.

Data Acquisition

To gather the data from the apparatus, from which calculations and manipulations are made, a Hewlett Packard 3497A (HP 3497A) Data Logger is used. There are two main tasks for this system: data acquisition and control as shown by Fig. 19.

The HP 3497 can be used for data acquisition and control; however, it is implemented in the experiment as just a data acquisition unit. The role of the data acquisition task is to measure data inputs from the system. For the HP 3497A, data acquisition measurements are divided into five categories, depending on the system parameter to be measured: voltage, temperature, resistance, frequency or pressure measurements.

In the data acquisition system shown, a transducer in the form of thermocouples is connected to the system and samples the system parameter temperature. The transducer converts the system physical parameter inputs into electrical signals (voltage) which can be measured by the HP 3497A via the interface bus. Measurements and data are then transferred and processed for storage and display.

The HP 3497A provides communications capabilities for direct connection or long distance communication. The HP 3497A is compatible with serial data (RS 232) interfaces as well as modems for connection over telephone lines.

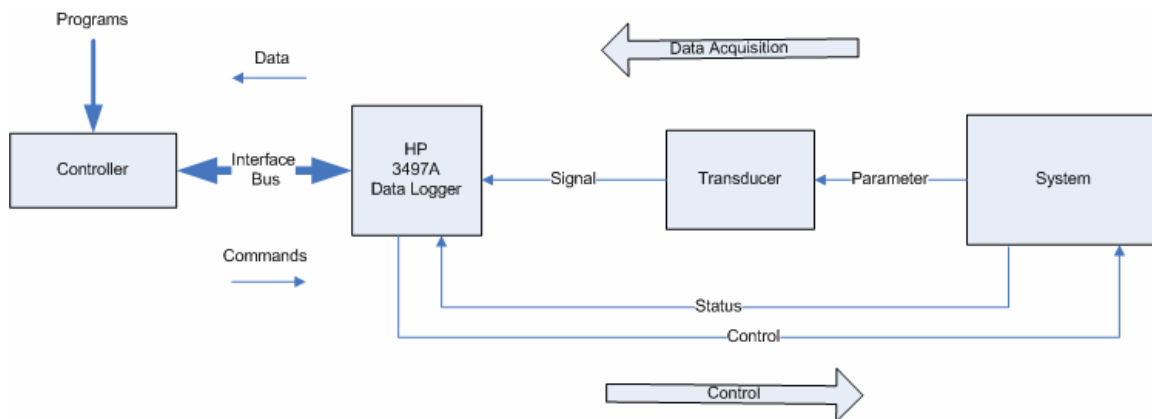


Fig. 19: Data Acquisition/Control System

A gauge controller powers as many as 13 pressure transducers simultaneously, allowing for switching instantly to any desired pressure measuring position. It has plug-in boards for Bayard-Alpert ion gauges, UHV ion gauges, cold cathode gauges, capacitance manometers, convection gauges and thermocouple gauges. It also has boards for RS232/RS485 interfacing, set points for automatic system pump down and protection, and remote I/O interconnection.

The chassis has five slots for sensor boards, many of which work with multiple sensors and one slot for the RS232/RS485 interface board. It will operate up to three high-vacuum gauges in any combination of Bayard-Alpert, true UHV or cold cathode sensors; up to eight thermocouple or convection gauge heads; and up to four capacitance manometers. The front panel controls and monitors all operating conditions except the main power switch. The gauge displays pressure in units of Torr down to 1.0×10^{-4} .

In summary, the two test plans attempted to simulate several possible design configurations, which would minimize the thermal energy transfer across the joint, and thus maximize the thermal insulation property of the Interstitial Insulating Coaxial Pipe.

RESULTS AND DISCUSSIONS

The experimental results compare the overall thermal joint resistance or equivalent heat transfer coefficient to the interface pressure and temperature. The lowest value for the equivalent heat transfer coefficient is needed to maximize the insulation capability of the mesh screen. Figure 20 shows the results for all the mesh sizes for the stainless steel wire screen specimens. As shown in Fig. 20, the lowest equivalent heat transfer coefficient was the stainless steel 5 mesh controlled at an interface temperature of 39 F and interface pressure approaching 175 kPa (25 psi). At the higher pressures, the results tend to converge due to the decrease in air gap distance where the thermal contact conductance dominates.

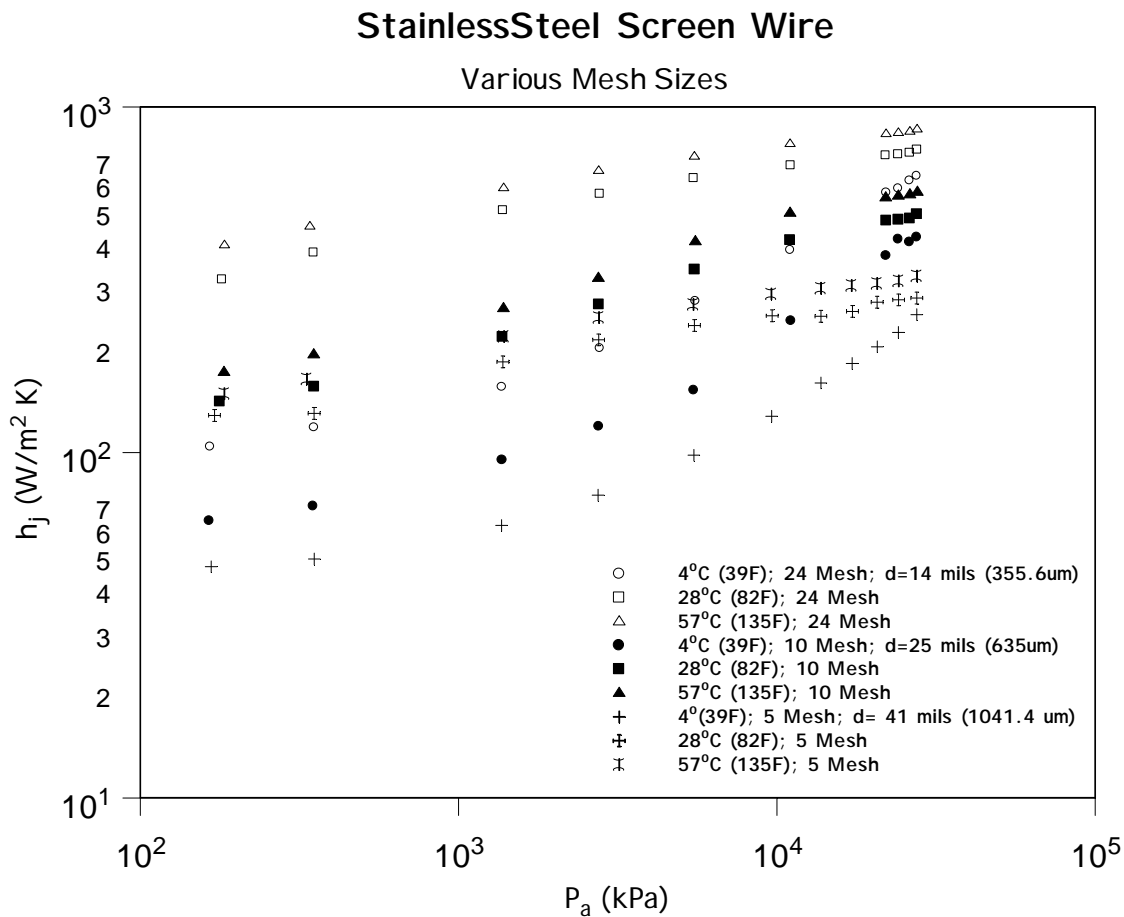


Fig. 20: Test results for the stainless steel wire mesh.

One observation which was noticed during testing was how the specimen was loaded (compressed) due to the higher pressures once the next interface temperature was run. Specimens were measured both prior and after a test run and a notable decrease in thickness was found. This meant that the specimens were being deformed at higher pressures. To limit this preloading effect, fresh specimens were entered in the test column for each new test run. Figure 21 compares the stainless steel 5 mesh with the titanium mesh specimens. From Fig. 21, the stainless steel 5 mesh out-performed the best of the titanium samples, which was the titanium 9 mesh. However, since the titanium 9 wire mesh was the smallest mesh number available that could be tested it is hard to definitely conclude that the stainless steel is better than the titanium. But at higher interface pressures an extrapolation of the data would indicate that stainless steel 5 mesh would still perform better with respect to lower thermal conductance. It must be indicated that the cost of titanium wire screen will be considerably higher than stainless steel wire without any significant improvement in insulating performance.

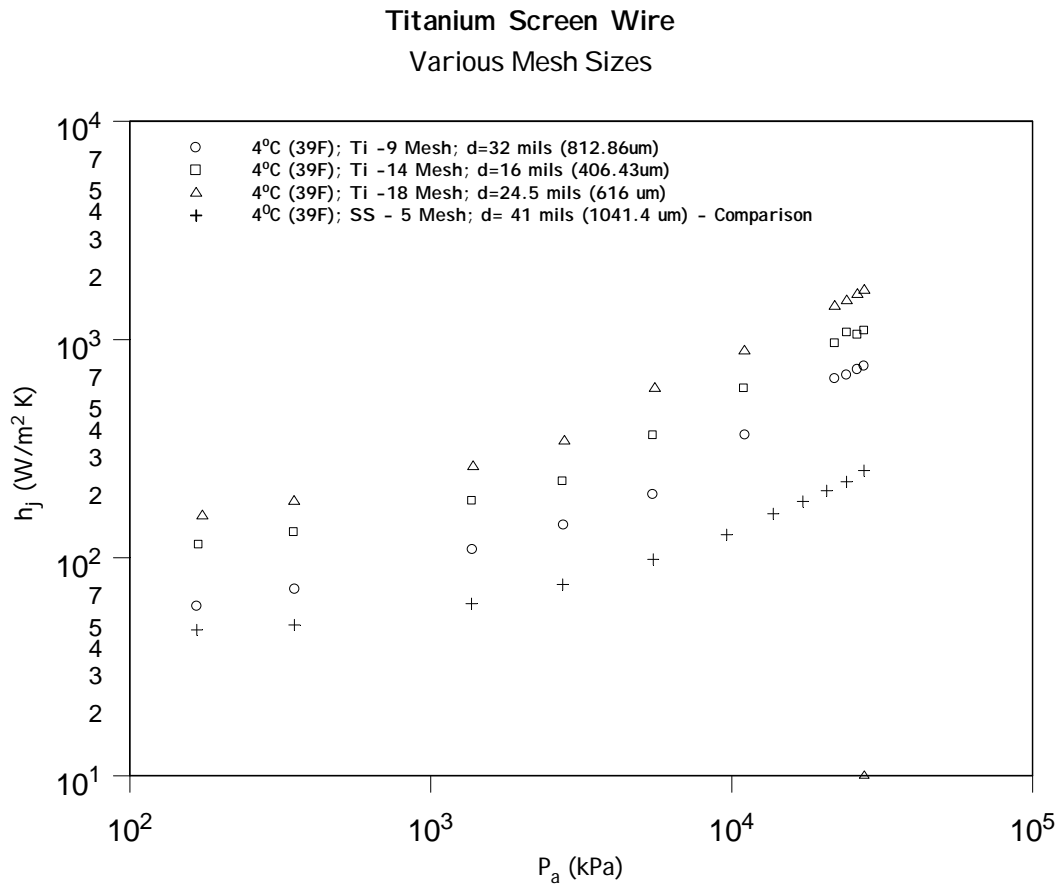


Fig. 21: Results of the Titanium mesh specimens compared to the Stainless Steel 5 mesh.

Both titanium and stainless steel materials have similar thermal conductivity with stainless steel having a value of 16.3 W/m-K (9.4 Btu/hr ft °F) and titanium equal to 17 W/m-K (9.8 Btu/hr ft °F). For purposes of this investigation, the stainless steel 5 mesh will be compared to the rest of the data. Figure 22 gives the results of the tungsten specimens and compares them to the stainless steel 5 mesh. Stainless steel 5 mesh out performed tungsten, which was expected due to tungsten's higher thermal conductivity value of 163.3 W/m-K (94.39 Btu/hr ft °F), an order of magnitude higher than the stainless steel material. Once the best mesh specimen was determined, it was tested in a composite assembly similar to a manufactured pipe. The stainless steel 5 mesh was tested between 2 samples of P110 4140 to show how the mesh will be used. The total thickness of this composite pipe wall was 19 mm (0.75 in). Also a sample of P110 4140, 19 mm (0.75 in) in thickness, without the wire mesh was tested to compare how the wire mesh directly affects the equivalent heat transfer coefficient.

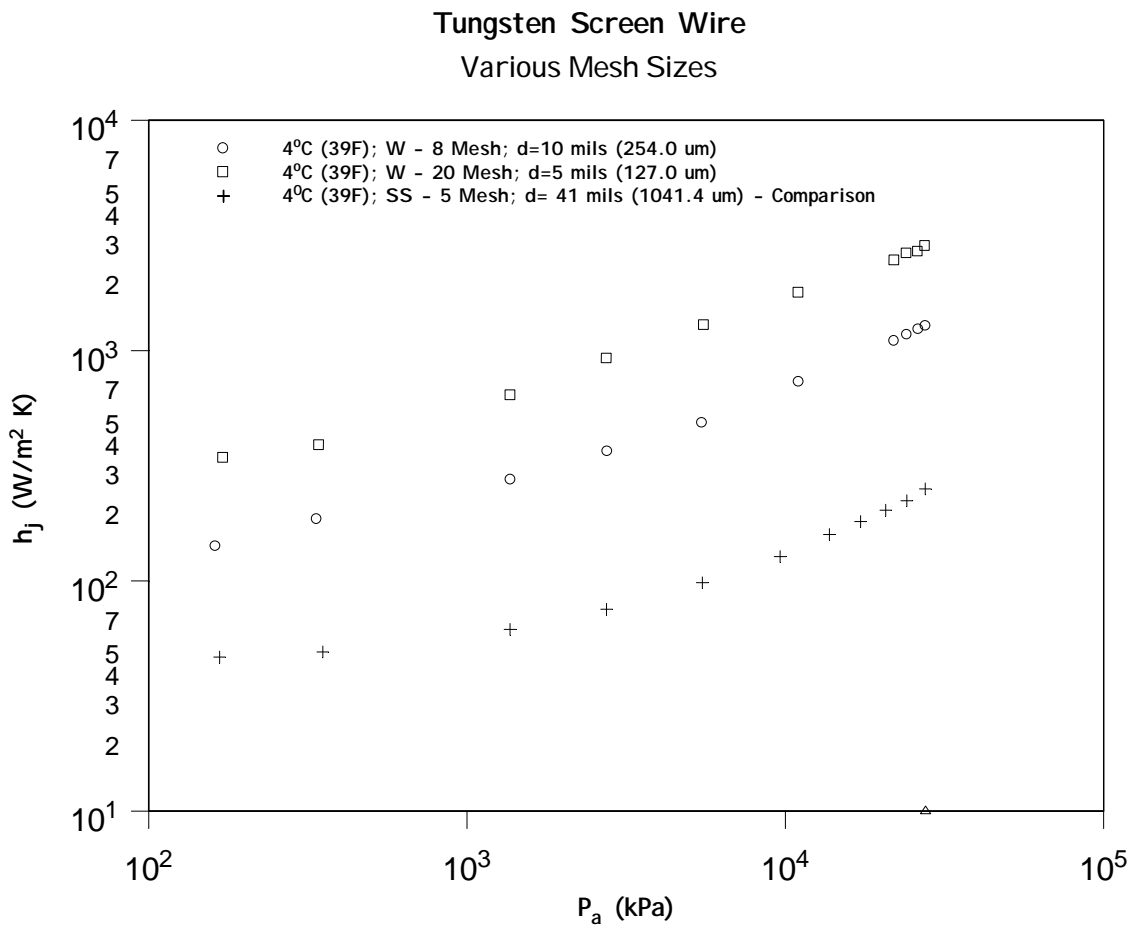


Fig. 22: Tungsten wire mesh specimens compared to the Stainless Steel 5 mesh.

Also, a sheet of Mylar film was added to the wire mesh tests to determine how the mesh would affect the results. Figure 23 presents the results of this test with a comparison to existing pipe technology currently in use. The experimental data show two orders of magnitude reduction in thermal contact conductance with stainless steel wire screen placed in-between the tubular pipe steel with *equivalent* thickness. This is defined as the tubular pipe thickness without the wire screen inserted, *e.g.*, 19 mm (0.748 in). This represents a very large reduction in the pipe thermal conductivity when the stainless steel 5 mesh wire screen was inserted at the center of the pipe. Moreover, a further 20% reduction in thermal conductance was realized when a sheet of thin (~12 μm thick (4.7×10^{-4} in)) Mylar film was placed at the two interfaces encompassed by the wire mesh contact points and the solid pipe metal. From Fig. 23, the best combination was the stainless steel 5 mesh with Mylar film in the assembly controlled at a mean interface temperature of 14.7°C (57.5 F). The value for the joint heat transfer coefficient at 167 kPa is 42.5 W/m²-K (7.48 Btu/ hr ft² °F), and it increases to a value of 67.4 W/m²K (11.9 Btu/hr ft² °F) at 3447 kPa (500 psi).

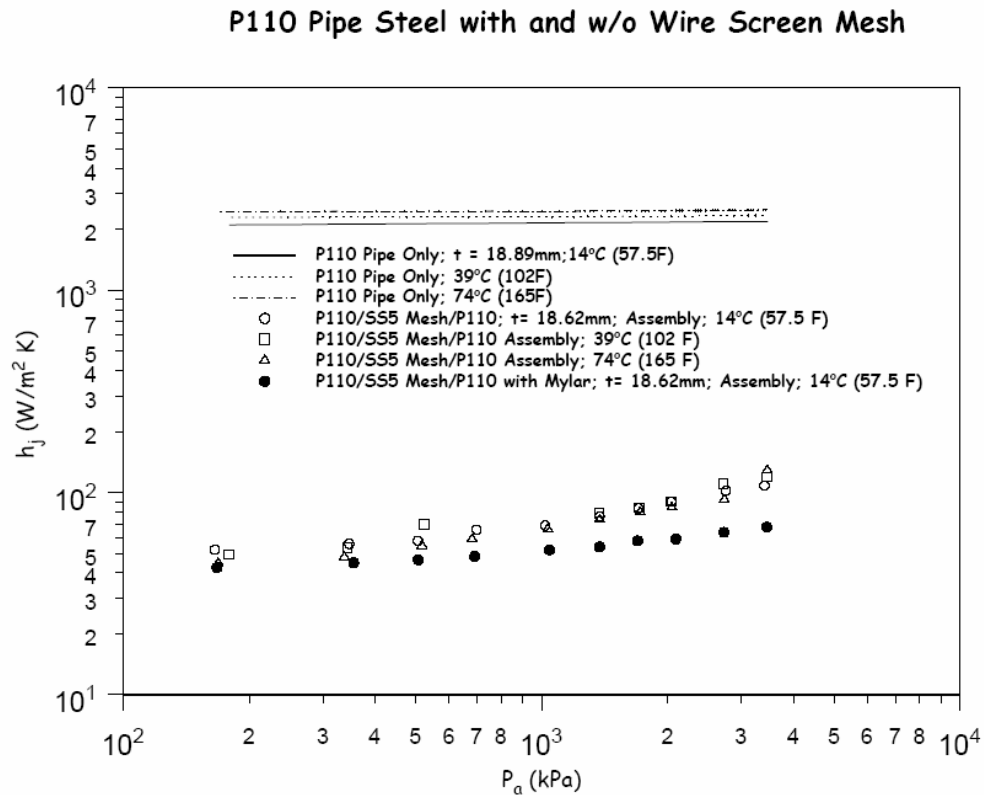


Fig. 23: Assembly test results compared to existing pipe.

The results for experimental runs for Inconel are shown in Fig. 24 as a function of applied interface pressure and average interface temperatures. A successions of configurations were tested which included a solid P110 pipe, P110 pipe with a roughened surface at the interface, and then P110 pipe inserts with an Inconel wire screen placed in between the two inserts. The latter configuration simulates the Interstitially Insulating Coaxial Pipe technology as envisioned, but unlike prior test runs, the test coupons held Inconel wire screen rather than the other material types mentioned earlier. Each set of experimental data shows the reduction in thermal joint conductance as the solid pipe is first divided into two halves with a fairly smooth surface ($R_{rms} \leq 1.0 \mu\text{m}$), the texturing of the contacting surfaces of the two inserts to increase surface roughness, and then the addition/placement of the wire screen to form a controlled air gap between the two P110 inserts. In each case there was a reduction in thermal joint conductance by one order of magnitude.

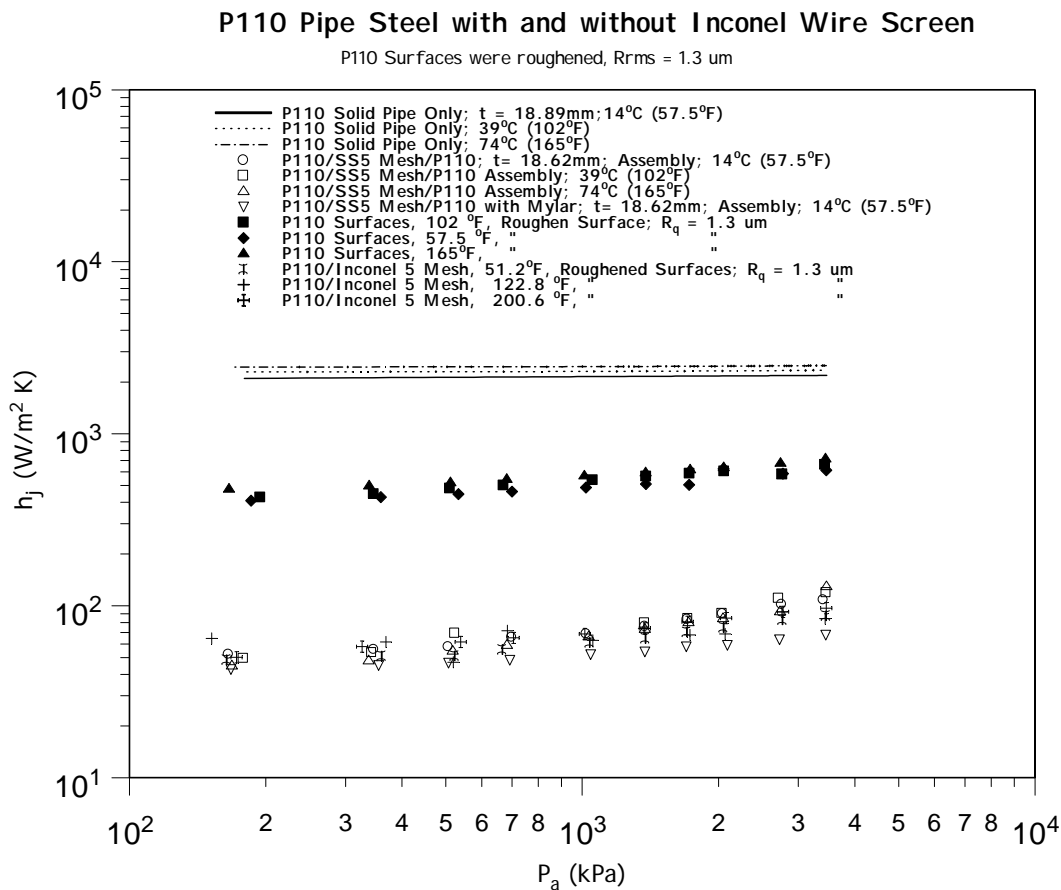


Fig. 24: Assembly test results with Inconel compared to existing P110 solid pipe and P110 roughened pipe interface.

The viability of a wire screen mesh as an insulation technology has been proven in this investigation as shown in Fig 25. The reduction in pipe effective thermal conductivity coefficient, k_{pipe} , from P110-4140 to the use of a wire mesh with Mylar dropped from 45 W/m-K (26 Btu/hr ft °F) to 0.08 W/m-K (0.05 Btu/hr ft °F). This is a large reduction in pipe thermal conductivity coefficient, $k_{wire/gap}$, which is a direct result of the very low thermal conductivity coefficient of the wire mesh/air-gap assembly (less than 0.72 W/m-K (0.42 Btu/hr ft °F), and which is compared against a insulation pipe technology solution, *e.g.* Fig. 3, currently employed by the oil industry. The effective thermal conductivity of the wire screen mesh can be computed from the measured thermal joint conductance, h_j , and the thickness of the wire screen mesh used in the experimental run. The following expression depicts this:

$$\frac{Q \cdot t}{A_c \cdot \Delta T} = h_j \cdot t = k_e \quad \frac{W}{m \cdot K} \quad (24)$$

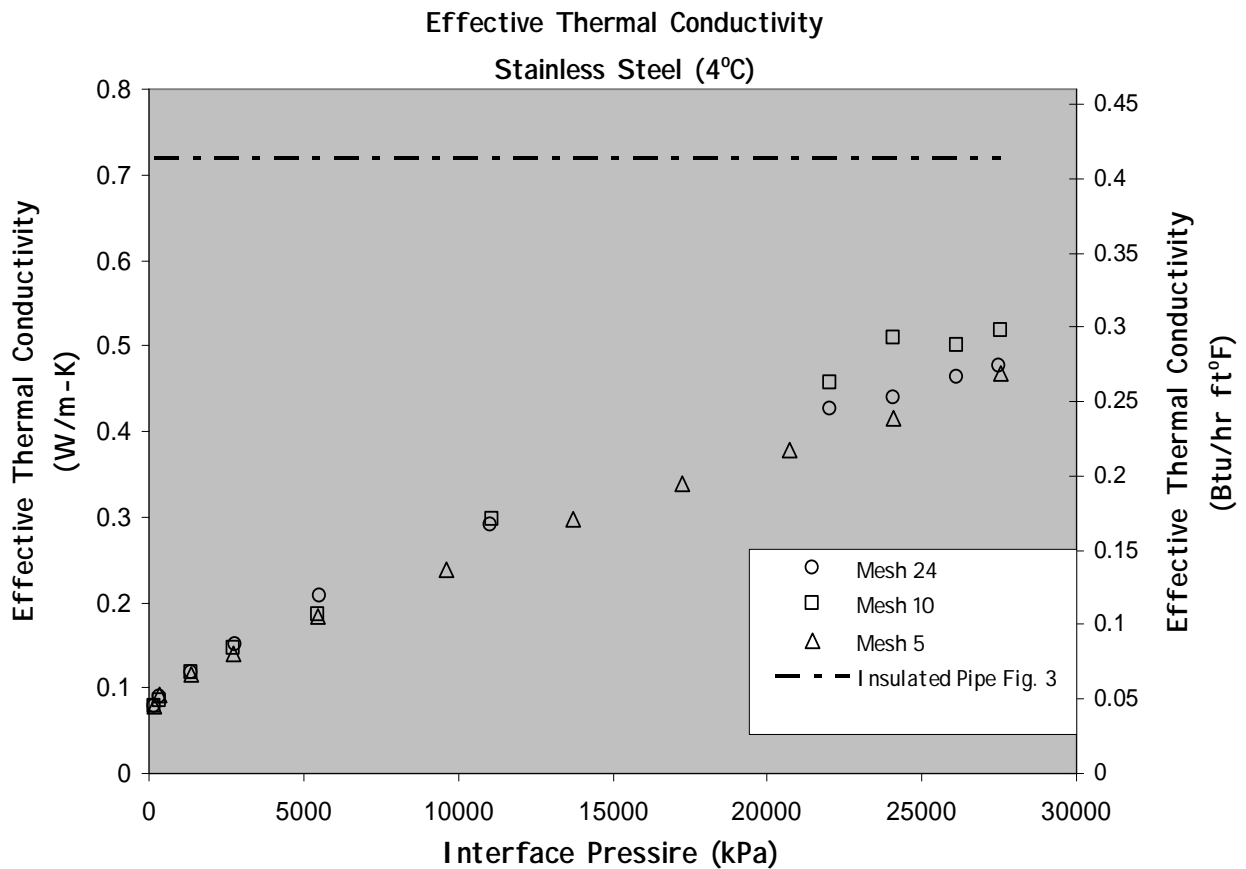


Fig. 25: Effective thermal conductivity, k_e , for the SS mesh numbers as a function of interface pressure and compared against the insulated pipe in Fig. 3.

CONCLUSIONS

This project investigates how an interstitially insulated coaxial pipe with a metal wire mesh can provide improved insulation properties with simplified pipe construction and production issues. By increasing the thermal contact resistance within the sub-sea pipe wall itself, the thermal energy leaving the oil and entering the cold sub-sea environment is decreased. Experiments have been conducted to measure the heat transfer conductance coefficient for this proposed technology and the results have been compared to current existing insulation technologies.

Different wire mesh materials have been tested, which include stainless steel, titanium, tungsten, and Inconel. Along with varying the material, the mesh number was varied, and thus, determining its effect on the overall thermal joint conductance. Moreover, a Mylar film was added to the test matrix as an additional layer of insulation/resistance. It was observed that a 5 mesh stainless steel wire screen with a Mylar film inserted at the two contacting interfaces provided the best insulation characteristics. The thermal conductance of the air/wire screen was experimentally measured as low as $42.5 \text{ W/m}^2\text{-K}$ ($7.48 \text{ Btu/hr ft}^2 \text{ }^\circ\text{F}$), which translates to an effective thermal conductivity of 0.08 W/m-K ($0.05 \text{ Btu/hr ft }^\circ\text{F}$), at an interface pressure of 172.3 kPa (25 psi). These values compare very favorably with current insulating materials whose effective thermal conductivity range from 0.12 to 0.15 W/m-K (0.07 to $0.09 \text{ Btu/hr ft }^\circ\text{F}$). The results seem to indicate superior insulating characteristics when compared to current technologies which have far greater complexity in construction, and show promise for sub-sea piping and oil/gas related applications. The viability of a wire mesh as insulating technology has been proven in this investigation.

Further, an order of magnitude decrease in the thermal conductivity, k , of P110-4140 pipe was observed with the use of a wire mesh/Mylar film conductor; the measured decrease was 45.0 W/m-K to 0.08 W/m-K (26.0 to $0.05 \text{ Btu/hr ft }^\circ\text{F}$). Interface pressure was also investigated to observe its affects on the heat transfer coefficient with the wire mesh present. As the pressure increases, the heat transfer coefficient also increases. The properties of the wire mesh include the number of contacts, mechanical properties, and geometry. These factors will all affect the insulating characteristics of the wire screen mesh.

REFERENCES

- ¹“Sub-sea Insulation.” *World Pipelines* May 2004: pp. 49-54.
- ²Choqueuse, Dominique, Angele Chomard and Christian Bucherie. “Insulation Materials for Ultra Deep Sea Flow Assurance: Evaluation of the Material Properties.” OTC14115 (2002): pp. 1-8.
- ³Hallot, Raymond, Angele Chomard and Stephane Couprie. “Ils – A Passive Insulation Solution To Answer Cool Down Time Challenges On Deep Water Flowlines.” OTC 14117 (2002): pp. 1-10.
- ⁴Cengel, Yunus. Heat Transfer: A Practical Approach. New York: McGraw Hill, 2003.
- ⁵Cividino, S., M. M. Yovanovich, and Fletcher, L. S., “A Model for Predicting the Joint Conductance of a Woven Wire Screen Contacting Two Solids.” *AIAA/ASME Thermophysics and Heat Transfer Conference 74-695* (July, 15 1974): pp. 1-17.
- ⁶Marks’ Standard Handbook for Mechanical Engineers.

Appendices

Appendix A – Thermal Experimental Data

Appendix B – Uncertainty

Appendix C – Wire Screen Literature

Appendix D – Tables in English Units

APPENDIX A- THERMAL EXPERIMENTAL DATA

Raw Data for 5 Mesh Stainless Steel					
Pressure (kPa)	Temperature (53°F)	Pressure (kPa)	Temperature (116°F)	Pressure (kPa)	Temperature (200°F)
166.91	46.70	170.91	128.00	183.36	148.20
351.99	49.15	351.50	129.89	333.88	163.22
1365.93	61.54	1378.34	183.04	1388.03	216.90
2745.52	75.33	2755.55	211.91	2757.11	245.83
5484.51	98.25	5505.09	233.50	5461.12	268.66
9615.79	127.37	9657.55	248.80	9597.11	287.93
13741.63	159.03	13737.10	248.30	13744.30	298.92
17231.23	181.22	17267.50	256.40	17168.40	304.69
20692.73	202.57	20656.80	272.70	20647.20	309.08
24094.84	222.87	24113.10	276.80	24121.30	314.40
27533.23	250.67	27529.90	280.30	27540.00	324.36

Raw Data for 10 Mesh Stainless Steel							
Pressure (kPa)	Temperature (53°F)	Pressure (kPa)	Temperature (116°F)	Pressure (kPa)	Temperature (200°F)	Pressure (kPa)	Temperature (116°F)
164.77	63.43	177.73	140.35	183.02	171.07	210.12	74.99
349.77	69.89	351.43	155.05	351.07	192.30	332.07	76.53
1370.66	95.05	1374.87	216.05	1382.81	261.77	1383.79	96.45
2756.49	119.01	2756.50	268.52	2749.75	320.37	2741.97	131.41
5478.62	151.45	5517.74	338.88	5541.56	409.07	5486.86	162.93
11073.40	240.65	11005.50	412.20	10994.80	494.46	8320.16	213.57
22014.30	371.43	22050.70	469.12	21994.80	547.87	13821.30	316.60
24090.90	414.15	24100.10	472.49	24077.90	553.74	20618.20	407.12
26133.10	406.70	26179.70	476.23	26178.00	558.86	24065.90	446.45
27530.60	419.91	27516.50	489.53	27600.80	568.44	27511.80	494.15

Raw Data for 24 Mesh Stainless Steel					
Pressure (kPa)	Temperature (53°F)	Pressure (kPa)	Temperature (116°F)	Pressure (kPa)	Temperature (200°F)
165.80	104.00	180.73	316.77	183.80	398.45
351.65	118.18	350.61	378.81	341.36	451.21
1367.97	154.73	1380.51	502.48	1385.89	582.87
2780.26	200.29	2777.62	560.95	2753.35	653.73
5546.56	274.60	5488.18	622.86	5504.50	719.67
11025.90	385.33	11064.00	678.19	10993.00	783.11
22046.80	565.07	21997.00	724.42	22027.10	836.58
24096.20	581.18	24079.70	729.81	24086.00	841.88
26134.30	612.76	26151.80	736.83	26158.30	848.86
27519.90	632.15	27571.60	752.39	27572.70	862.07

Raw Data for 9 Mesh Titanium		Raw Data for 14 Mesh Titanium		Raw Data for 18 Mesh Titanium	
Pressure (kPa)	Temperature (4°F)	Pressure (kPa)	Temperature (4°F)	Pressure (kPa)	Temperature (53°F)
166.83	59.86	169.54	114.52	174.05	155.91
353.27	71.66	350.99	130.76	351.30	181.78
1374.22	108.84	1373.58	182.21	1382.09	261.88
2765.50	141.07	2743.94	223.57	2778.41	343.04
5471.12	194.75	5485.39	363.52	5555.67	598.04
11071.80	365.26	10971.10	597.10	11023.00	888.94
22013.30	661.94	22037.00	961.15	21994.60	1424.40
24121.90	687.86	24172.80	1077.13	24132.00	1508.16
26198.00	729.47	26172.40	1051.90	26164.20	1612.19
27570.50	755.96	27579.70	1099.32	27594.00	1684.74

Raw Data for 8 Mesh Tungsten		Raw Data for 20 Mesh Tungsten	
Pressure (kPa)	Temperature (4°F)	Pressure (kPa)	Temperature (4°F)
161.98	141.35	171.30	341.91
337.31	185.53	343.08	388.09
1370.47	274.97	1369.69	638.92
2761.04	364.57	2748.63	923.70
5468.19	485.12	5555.08	1287.64
11016.70	730.76	10993.70	1782.53
22000.50	1102.22	22038.30	2462.83
24118.10	1170.16	24077.90	2637.14
26173.70	1237.45	26140.80	2688.24
27549.60	1278.66	27520.60	2840.65

Raw Data for 5 Mesh Stainless Steel with Mylar					
Pressure (kPa)	Temperature (53°F)	Pressure (kPa)	Temperature (116°F)	Pressure (kPa)	Temperature (200°F)
178.26	37.37	178.92	34.16	171.46	57.01
356.53	36.05	338.83	39.67	348.88	61.70
525.83	39.07	507.79	46.29	516.11	64.99
701.83	40.42	680.38		690.49	69.02
1052.85	40.18	1046.43	59.61	1023.19	74.90
1392.95	41.48	1359.02		1365.94	80.69
1730.00	47.07	1709.85	71.71	1742.28	87.02
2105.62	53.47	2044.67		2092.70	90.40
2776.84	56.76	2745.26		2761.87	95.66
3421.24	62.17	3410.75	84.69	3385.48	102.64

Raw Data for P110 4140 Steel 19mm Insert					
Pressure (kPa)	Temperature (53°F)	Pressure (kPa)	Temperature (135°F)	Pressure (kPa)	Temperature (200°F)
179.29	2084.95	181.68	2277.30	170.80	2435.63
343.78	2095.18	338.30	2291.17	351.28	2445.25
512.09	2097.08	506.22	2298.32	519.04	2448.74
690.97	2200.90	686.14	2301.56	697.75	2457.41
1038.95	2204.62	1033.64	2308.90	1022.30	2460.74
1373.48	2205.18	1371.60	2318.70	1382.56	2470.15
1746.56	2116.71	1693.32	2322.58	1722.97	2472.42
2053.21	2132.75	2070.50	2324.01	2047.72	2474.59
2803.84	2229.33	2713.54	2329.84	2731.27	2481.02
3465.05	2133.33	3406.06	2334.06	3458.93	2487.04

Raw Data for 5 Mesh Stainless Steel with P110 Assembly					
Pressure (kPa)	Temperature (53°F)	Pressure (kPa)	Temperature (135°F)	Pressure (kPa)	Temperature (200°F)
165.39	52.17	178.45	49.32	168.45	44.76
346.40	55.72	342.85	53.42	337.55	47.99
505.90	57.70	523.45	69.34	517.10	54.63
698.54	65.55	686.80		681.72	58.97
1020.51	68.54	1015.70		1033.82	66.11
1376.13	75.88	1374.37	79.40	1375.52	73.32
1706.73	83.32	1712.37	84.09	1715.75	79.89
2040.19	89.97	2035.89	90.28	2046.36	84.40
2755.90	101.72	2714.48	110.31	2733.90	92.43
3406.90	108.23	3456.27	119.04	3464.39	129.30

Raw Data for 5 Mesh Stainless Steel and Mylar with P110	
Pressure (kPa)	Temp. (53°F)
167.45	42.58
354.94	44.97
506.75	46.46
691.93	48.24
1043.45	52.02
1375.59	53.81
1696.64	57.64
2092.05	58.76
2727.93	63.48
3447.83	67.43

Set #1 Test @ 290K	
Pressure (Pa)	Conductance (W/m²-K)
165980.65	969.914359
356855.456	991.549585
499206.507	996.8211667
671862.849	1005.499647
1379075.519	1050.723066
1713888.427	1050.482035
2071464.387	1073.038875
2742474.395	1084.894032
3455920.631	1119.433373

Set #1 Test @ 320K	
Pressure (Pa)	Conductance (W/m²-K)
149967.811	1228.553194
355473.264	1241.436272
508161.346	1270.105258
668216.216	1280.823308
1058950.075	1318.172201
1384779.736	1341.544972
1711359.31	1362.786541
2056039.715	1383.425639
2772764.981	1416.475605
3439113.767	1443.446427

Set #1 @ 360K	
Pressure (Pa)	Conductance (W/m²-K)
170230.154	1336.647671
320977.286	1343.158954
533393.698	1375.699518
682288.105	1392.188749
1021395.63	1424.38644
1388485.186	1459.679087
1725342.974	1482.012145
2061127.357	1487.742608
2778470.198	1530.76771
3461199.428	1555.520759

Set #2 @ 290K	
Pressure (Pa)	Conductance (W/m²-K)
185743.052	408.417234
359252.235	428.331477
532629.082	446.354321
699712.544	461.823233
1019660.538	487.419274
1381750.677	509.956667
1721887.494	505.107907
2050040.414	627.053217
2773279.627	586.7037702
3457023.444	613.345775

Set #2 @ 320K	
Pressure (Pa)	Conductance (W/m²-K)
194359.694	427.063651
346253.751	447.046401
510205.225	480.40511
669892.491	500.232404
1053935.945	537.157256
1384706.215	564.47275
1727225.107	586.626851
2059333.448	604.365359
2764207.155	581.098339
3435246.571	658.813437

Set #2 @ 360K	
Pressure (Pa)	Conductance (W/m²-K)
165892.425	477.333812
338239.979	498.980847
511793.275	520.737958
680729.463	543.817421
1011161.529	569.820881
1380809.611	595.406193
1732327.454	618.927376
2054539.889	637.502421
2738945.394	674.33814
3446642.301	716.651111

APPENDIX B- UNCERTAINTY ANALYSIS

Uncertainty Analysis (5 Mesh Stainless Steel @53°F and 24.2 PSI)

Uncertainty in Temperature Measurement from K-Type Thermocouples

$$\Delta T_1 = \pm 0.5^\circ\text{C}$$

$$\Delta T_2 = \pm 0.5^\circ\text{C}$$

Uncertainty in Area

$$A = \frac{\pi}{4} D^2 \qquad \frac{dA}{dD} = \frac{\pi}{2} D \cdot \Delta D$$

Values

$$\Delta D = 2 \text{ mil} = .002 \text{ inch} = 0.0000508 \text{ m}$$

$$D = 1 \text{ inch} = 0.0254 \text{ m}$$

$$\omega_A = \sqrt{\left(\frac{dA}{dD} \cdot \Delta D\right)^2} = \sqrt{\left(\frac{\pi}{2}(0.0254)(0.0000508)\right)^2} = 0.000002027 \text{ m}^2$$

Uncertainty in thermal conductivity, k

$$\Delta k = \pm 0.0049 \text{ W/mK}$$

$$k = 0.081 \text{ W/mK}$$

$$A = 0.00486 \text{ m}^2$$

$$L = 0.001905 \text{ m}$$

$$\Delta L = 0.0000508 \text{ m}$$

Uncertainty in \dot{Q}

$$\dot{Q} = \frac{kA}{L}(T_1 - T_2)$$

$$\frac{d\dot{Q}}{dk} = \frac{A}{L}(T_1 - T_2) \cdot \Delta k = \frac{0.0005067}{0.001905}(17.23 - -7.75) \cdot 0.00486 = 0.0323$$

$$\frac{d\dot{Q}}{dA} = \frac{k}{L}(T_1 - T_2) \cdot \Delta A = \frac{0.081}{0.001905}(17.23 - -7.75) \cdot 0.000002027 = 0.0022$$

$$\frac{d\dot{Q}}{dL} = \frac{kA}{L^2}(T_2 - T_1) \cdot \Delta L = \frac{0.081(0.0005067)}{(0.001905)^2}(-7.75 - 17.23) \cdot 0.0000508 = -0.0144$$

$$\frac{d\dot{Q}}{dT_1} = \frac{kA}{L} \cdot \Delta T_1 = \frac{0.081(0.0005067)}{0.001905} \cdot 0.5 = 0.0108$$

$$\frac{d\dot{Q}}{dT_2} = -\frac{kA}{L} \cdot \Delta T_2 = -\frac{0.081(0.0005067)}{0.001905} \cdot 0.5 = -0.0108$$

$$\omega_{\dot{Q}} = \sqrt{\left(\frac{d\dot{Q}}{dk} \cdot \Delta k\right)^2 + \left(\frac{d\dot{Q}}{dA} \cdot \Delta A\right)^2 + \left(\frac{d\dot{Q}}{dL} \cdot \Delta L\right)^2 + \left(\frac{d\dot{Q}}{dT_1} \cdot \Delta T_1\right)^2 + \left(\frac{d\dot{Q}}{dT_2} \cdot \Delta T_2\right)^2} =$$

$$\sqrt{(0.0323)^2 + (0.0022)^2 + (-0.0144)^2 + (0.0108)^2 + (-0.0108)^2}$$

$$= 0.039 \text{ W}$$

Uncertainty in the heat transfer coefficient, h

$$h = \frac{\dot{Q}/A}{T_1 - T_2}$$

$$\frac{dh}{dQ} = \frac{1}{A(T_1 - T_2)} \cdot \Delta Q = \frac{1}{0.0005067(17.23 - -7.75)} \cdot 0.039 = 3.0812$$

$$\frac{dh}{dA} = -\frac{\dot{Q}}{A^2(T_1 - T_2)} \cdot \Delta A = -\frac{0.54}{0.0005067^2(17.23 - -7.75)} \cdot 0.000002027 = -0.17067$$

$$\frac{dh}{dT_1} = -\frac{\dot{Q}}{A(T_1 - T_2)^2} \cdot \Delta T_1 = -\frac{0.54}{0.0005067(17.23 - -7.75)^2} \cdot 0.5 = -0.854$$

$$\frac{dh}{dT_2} = \frac{\dot{Q}}{A(T_1 - T_2)^2} \cdot \Delta T_2 = \frac{0.54}{0.0005067(17.23 - -7.75)^2} \cdot 0.5 = 0.854$$

$$\omega_h = \sqrt{\left(\frac{dh}{d\dot{Q}} \cdot \Delta \dot{Q}\right)^2 + \left(\frac{dh}{dA} \cdot \Delta A\right)^2 + \left(\frac{dh}{dT_1} \cdot \Delta T_1\right)^2 + \left(\frac{dh}{dT_2} \cdot \Delta T_2\right)^2} =$$

$$= \sqrt{(3.0812)^2 + (-0.17067)^2 + (-0.854)^2 + (0.854)^2} = 3.31 \text{ W/m}^2\text{K}$$

Therefore,

$$h = 42.695 \pm 3.31 \text{ W/m}^2\text{K}$$

$$\% \text{Error} = \frac{3.31}{42.695} \cdot 100\% = 7.75\%$$

Uncertainty Analysis (5 Mesh Stainless Steel @53°F and 198.1 PSI)

Uncertainty in Temperature Measurement from K-Type Thermocouples

$$\Delta T_1 = \pm 0.5^\circ\text{C}$$

$$\Delta T_2 = \pm 0.5^\circ\text{C}$$

Uncertainty in Area

$$A = \frac{\pi}{4} D^2 \qquad \frac{dA}{dD} = \frac{\pi}{2} D \cdot \Delta D$$

Values

$$\Delta D = 2 \text{ mil} = .002 \text{ inch} = 0.0000508 \text{ m}$$

$$D = 1 \text{ inch} = 0.0254 \text{ m}$$

$$\omega_A = \sqrt{\left(\frac{dA}{dD} \cdot \Delta D\right)^2} = \sqrt{\left(\frac{\pi}{2} (0.0254)(0.0000508)\right)^2} = 0.000002027 \text{ m}^2$$

Uncertainty in thermal conductivity, k

$$\Delta k = \pm 0.007 \text{ W/mK}$$

$$k = 0.12 \text{ W/mK}$$

$$A = 0.0005067 \text{ m}^2$$

$$L = 0.001905 \text{ m}$$

$$\Delta L = 0.0000508 \text{ m}$$

Uncertainty in \dot{Q}

$$\dot{Q} = \frac{kA}{L} (T_1 - T_2)$$

$$\frac{d\dot{Q}}{dk} = \frac{A}{L} (T_1 - T_2) \cdot \Delta k = \frac{0.0005067}{0.001905} (16.48 - -7.16) \cdot 0.007 = 0.044$$

$$\frac{d\dot{Q}}{dA} = \frac{k}{L} (T_1 - T_2) \cdot \Delta A = \frac{0.12}{0.001905} (16.48 - -7.16) \cdot 0.000002027 = 0.003$$

$$\frac{d\dot{Q}}{dL} = \frac{kA}{L^2} (T_2 - T_1) \cdot \Delta L = \frac{0.12(0.0005067)}{(0.001905)^2} (-7.16 - 16.48) \cdot 0.0000508 = -0.0201$$

$$\frac{d\dot{Q}}{dT_1} = \frac{kA}{L} \cdot \Delta T_1 = \frac{0.12(0.0005067)}{0.001905} \cdot 0.5 = 0.016$$

$$\frac{d\dot{Q}}{dT_2} = -\frac{kA}{L} \cdot \Delta T_2 = -\frac{0.12(0.0005067)}{0.001905} \cdot 0.5 = -0.016$$

$$\omega_{\dot{Q}} = \sqrt{\left(\frac{d\dot{Q}}{dk} \cdot \Delta k\right)^2 + \left(\frac{d\dot{Q}}{dA} \cdot \Delta A\right)^2 + \left(\frac{d\dot{Q}}{dL} \cdot \Delta L\right)^2 + \left(\frac{d\dot{Q}}{dT_1} \cdot \Delta T_1\right)^2 + \left(\frac{d\dot{Q}}{dT_2} \cdot \Delta T_2\right)^2} =$$

$$\sqrt{(0.044)^2 + (0.003)^2 + (-0.0201)^2 + (0.016)^2 + (-0.016)^2}$$

$$= 0.053 \text{ W}$$

Uncertainty in the heat transfer coefficient, h

$$h = \frac{\dot{Q}/A}{T_1 - T_2}$$

$$\frac{dh}{dQ} = \frac{1}{A(T_1 - T_2)} \cdot \Delta Q = \frac{1}{0.0005067(16.48 - -7.16)} \cdot 0.053 = 4.42$$

$$\frac{dh}{dA} = -\frac{\dot{Q}}{A^2(T_1 - T_2)} \cdot \Delta A = -\frac{0.74}{0.0005067^2(16.48 - -7.16)} \cdot 0.000002027 = -0.2471$$

$$\frac{dh}{dT_1} = -\frac{\dot{Q}}{A(T_1 - T_2)^2} \cdot \Delta T_1 = -\frac{0.74}{0.0005067(16.48 - -7.16)^2} \cdot 0.5 = -1.307$$

$$\frac{dh}{dT_2} = \frac{\dot{Q}}{A(T_1 - T_2)^2} \cdot \Delta T_2 = \frac{0.74}{0.0005067(16.48 - -7.16)^2} \cdot 0.5 = 1.307$$

$$\omega_h = \sqrt{\left(\frac{dh}{d\dot{Q}} \cdot \Delta \dot{Q}\right)^2 + \left(\frac{dh}{dA} \cdot \Delta A\right)^2 + \left(\frac{dh}{dT_1} \cdot \Delta T_1\right)^2 + \left(\frac{dh}{dT_2} \cdot \Delta T_2\right)^2} =$$

$$= \sqrt{(4.42)^2 + (-0.2471)^2 + (-1.307)^2 + (1.307)^2} = 4.80 \text{ W/m}^2\text{K}$$

Therefore,

$$\mathbf{h = 61.54 \pm 4.80 \text{ W/m}^2\text{K}}$$

$$\mathbf{\%Error = \frac{4.80}{61.54} \cdot 100\% = 7.78\%}$$

Uncertainty Analysis (5 Mesh Stainless Steel @53°F and 398.21 PSI)

Uncertainty in Temperature Measurement from K-Type Thermocouples

$$\Delta T_1 = \pm 0.5^\circ\text{C}$$

$$\Delta T_2 = \pm 0.5^\circ\text{C}$$

Uncertainty in Area

$$A = \frac{\pi}{4} D^2 \qquad \frac{dA}{dD} = \frac{\pi}{2} D \cdot \Delta D$$

Values

$$\Delta D = 2 \text{ mil} = .002 \text{ inch} = 0.0000508 \text{ m}$$

$$D = 1 \text{ inch} = 0.0254 \text{ m}$$

$$\omega_A = \sqrt{\left(\frac{dA}{dD} \cdot \Delta D\right)^2} = \sqrt{\left(\frac{\pi}{2}(0.0254)(0.0000508)\right)^2} = 0.000002027 \text{ m}^2$$

Uncertainty in thermal conductivity, k

$$\Delta k = \pm 0.009 \text{ W/mK}$$

$$k = 0.144 \text{ W/mK}$$

$$A = 0.0005067 \text{ m}^2$$

$$L = 0.001905 \text{ m}$$

$$\Delta L = 0.0000508 \text{ m}$$

Uncertainty in \dot{Q}

$$\dot{Q} = \frac{kA}{L}(T_1 - T_2)$$

$$\frac{d\dot{Q}}{dk} = \frac{A}{L}(T_1 - T_2) \cdot \Delta k = \frac{0.0005067}{0.001905}(16.10 - -6.83) \cdot 0.009 = 0.0549$$

$$\frac{d\dot{Q}}{dA} = \frac{k}{L}(T_1 - T_2) \cdot \Delta A = \frac{0.144}{0.001905}(16.10 - -6.83) \cdot 0.000002027 = 0.0035$$

$$\frac{d\dot{Q}}{dL} = \frac{kA}{L^2}(T_2 - T_1) \cdot \Delta L = \frac{0.144(0.0005067)}{(0.001905)^2}(-6.83 - 16.10) \cdot 0.0000508 = -.0234$$

$$\frac{d\dot{Q}}{dT_1} = \frac{kA}{L} \cdot \Delta T_1 = \frac{0.144(0.0005067)}{0.001905} \cdot 0.5 = 0.0192$$

$$\frac{d\dot{Q}}{dT_2} = -\frac{kA}{L} \cdot \Delta T_2 = -\frac{0.144(0.0005067)}{0.001905} \cdot 0.5 = -0.0192$$

$$\omega_{\dot{Q}} = \sqrt{\left(\frac{d\dot{Q}}{dk} \cdot \Delta k\right)^2 + \left(\frac{d\dot{Q}}{dA} \cdot \Delta A\right)^2 + \left(\frac{d\dot{Q}}{dL} \cdot \Delta L\right)^2 + \left(\frac{d\dot{Q}}{dT_1} \cdot \Delta T_1\right)^2 + \left(\frac{d\dot{Q}}{dT_2} \cdot \Delta T_2\right)^2} =$$

$$\sqrt{(0.0549)^2 + (0.0035)^2 + (-0.0234)^2 + (0.0192)^2 + (-0.0192)^2}$$

$$= 0.066 \text{ W}$$

Uncertainty in the heat transfer coefficient, h

$$h = \frac{\dot{Q}/A}{T_1 - T_2}$$

$$\frac{dh}{dQ} = \frac{1}{A(T_1 - T_2)} \cdot \Delta Q = \frac{1}{0.0005067(16.10 - -6.83)} \cdot 0.066 = 5.681$$

$$\frac{dh}{dA} = -\frac{\dot{Q}}{A^2(T_1 - T_2)} \cdot \Delta A = -\frac{0.875}{0.0005067^2(16.10 - -6.83)} \cdot 0.000002027 = -0.3013$$

$$\frac{dh}{dT_1} = -\frac{\dot{Q}}{A(T_1 - T_2)^2} \cdot \Delta T_1 = -\frac{0.875}{0.0005067(16.10 - -6.83)^2} \cdot 0.5 = -1.642$$

$$\frac{dh}{dT_2} = \frac{\dot{Q}}{A(T_1 - T_2)^2} \cdot \Delta T_2 = \frac{0.875}{0.0005067(16.10 - -6.83)^2} \cdot 0.5 = 1.642$$

$$\omega_h = \sqrt{\left(\frac{dh}{d\dot{Q}} \cdot \Delta \dot{Q}\right)^2 + \left(\frac{dh}{dA} \cdot \Delta A\right)^2 + \left(\frac{dh}{dT_1} \cdot \Delta T_1\right)^2 + \left(\frac{dh}{dT_2} \cdot \Delta T_2\right)^2} =$$

$$= \sqrt{(5.681)^2 + (-0.3013)^2 + (-1.642)^2 + (1.642)^2} = 6.14 \text{ W/m}^2\text{K}$$

Therefore,

$$h = 75.33 \pm 6.14 \text{ W/m}^2\text{K}$$

$$\% \text{Error} = \frac{6.14}{75.33} \cdot 100\% = 8.15\%$$

Uncertainty Analysis (5 Mesh Stainless Steel @200°F and 26.6 PSI)

Uncertainty in Temperature Measurement from K-Type Thermocouples

$$\Delta T_1 = \pm 0.5^\circ\text{C}$$

$$\Delta T_2 = \pm 0.5^\circ\text{C}$$

Uncertainty in Area

$$A = \frac{\pi}{4} D^2 \qquad \frac{dA}{dD} = \frac{\pi}{2} D \cdot \Delta D$$

Values

$$\Delta D = 2 \text{ mil} = .002 \text{ inch} = 0.0000508 \text{ m}$$

$$D = 1 \text{ inch} = 0.0254 \text{ m}$$

$$\omega_A = \sqrt{\left(\frac{dA}{dD} \cdot \Delta D\right)^2} = \sqrt{\left(\frac{\pi}{2}(0.0254)(0.0000508)\right)^2} = 0.000002027 \text{ m}^2$$

Uncertainty in thermal conductivity, k

$$\Delta k = \pm 0.017 \text{ W/mK}$$

$$k = 0.28 \text{ W/mK}$$

$$A = 0.0005067 \text{ m}^2$$

$$L = 0.001905 \text{ m}$$

$$\Delta L = 0.0000508 \text{ m}$$

Uncertainty in \dot{Q}

$$\dot{Q} = \frac{kA}{L}(T_1 - T_2)$$

$$\frac{d\dot{Q}}{dk} = \frac{A}{L}(T_1 - T_2) \cdot \Delta k = \frac{0.0005067}{0.001905}(90.51 - 5.51) \cdot 0.017 = 0.3843$$

$$\frac{d\dot{Q}}{dA} = \frac{k}{L}(T_1 - T_2) \cdot \Delta A = \frac{0.28}{0.001905}(90.51 - 5.51) \cdot 0.000002027 = 0.0253$$

$$\frac{d\dot{Q}}{dL} = \frac{kA}{L^2}(T_2 - T_1) \cdot \Delta L = \frac{0.28(0.0005067)}{(0.001905)^2}(5.51 - 90.51) \cdot 0.0000508 = -0.1688$$

$$\frac{d\dot{Q}}{dT_1} = \frac{kA}{L} \cdot \Delta T_1 = \frac{0.28(0.0005067)}{0.001905} \cdot 0.5 = 0.0372$$

$$\frac{d\dot{Q}}{dT_2} = -\frac{kA}{L} \cdot \Delta T_2 = -\frac{0.28(0.0005067)}{0.001905} \cdot 0.5 = -0.0372$$

$$\omega_{\dot{Q}} = \sqrt{\left(\frac{d\dot{Q}}{dk} \cdot \Delta k\right)^2 + \left(\frac{d\dot{Q}}{dA} \cdot \Delta A\right)^2 + \left(\frac{d\dot{Q}}{dL} \cdot \Delta L\right)^2 + \left(\frac{d\dot{Q}}{dT_1} \cdot \Delta T_1\right)^2 + \left(\frac{d\dot{Q}}{dT_2} \cdot \Delta T_2\right)^2} =$$

$$\sqrt{(0.3834)^2 + (0.0253)^2 + (-0.1688)^2 + (0.0372)^2 + (-0.0372)^2}$$

$$= 0.423 \text{ W}$$

Uncertainty in the heat transfer coefficient, h

$$h = \frac{\dot{Q}/A}{T_1 - T_2}$$

$$\frac{dh}{dQ} = \frac{1}{A(T_1 - T_2)} \cdot \Delta Q = \frac{1}{0.0005067(90.51 - 5.51)} \cdot 0.423 = 9.8213$$

$$\frac{dh}{dA} = -\frac{\dot{Q}}{A^2(T_1 - T_2)} \cdot \Delta A = -\frac{6.38}{0.0005067^2(90.51 - 5.51)} \cdot 0.000002027 = -0.5926$$

$$\frac{dh}{dT_1} = -\frac{\dot{Q}}{A(T_1 - T_2)^2} \cdot \Delta T_1 = -\frac{6.38}{0.0005067(90.51 - 5.51)^2} \cdot 0.5 = -0.8714$$

$$\frac{dh}{dT_2} = \frac{\dot{Q}}{A(T_1 - T_2)^2} \cdot \Delta T_2 = \frac{6.38}{0.0005067(90.51 - 5.51)^2} \cdot 0.5 = 0.8714$$

$$\omega_h = \sqrt{\left(\frac{dh}{dQ} \cdot \Delta Q\right)^2 + \left(\frac{dh}{dA} \cdot \Delta A\right)^2 + \left(\frac{dh}{dT_1} \cdot \Delta T_1\right)^2 + \left(\frac{dh}{dT_2} \cdot \Delta T_2\right)^2} =$$

$$= \sqrt{(9.8213)^2 + (-0.5926)^2 + (-0.8714)^2 + (0.8714)^2} = 9.92 \text{ W/m}^2\text{K}$$

Therefore,

$$\mathbf{h = 148.21 \pm 9.92 \text{ W/m}^2\text{K}}$$

$$\% \text{Error} = \frac{9.92}{148.21} \cdot 100\% = 6.69\%$$

Uncertainty Analysis (5 Mesh Stainless Steel @ 200°F and 201.32 PSI)

Uncertainty in Temperature Measurement from K-Type Thermocouples

$$\Delta T_1 = \pm 0.5^\circ\text{C}$$

$$\Delta T_2 = \pm 0.5^\circ\text{C}$$

Uncertainty in Area

$$A = \frac{\pi}{4} D^2 \qquad \frac{dA}{dD} = \frac{\pi}{2} D \cdot \Delta D$$

Values

$$\Delta D = 2 \text{ mil} = .002 \text{ inch} = 0.0000508 \text{ m}$$

$$D = 1 \text{ inch} = 0.0254 \text{ m}$$

$$\omega_A = \sqrt{\left(\frac{dA}{dD} \cdot \Delta D\right)^2} = \sqrt{\left(\frac{\pi}{2}(0.0254)(0.0000508)\right)^2} = 0.000002027 \text{ m}^2$$

Uncertainty in thermal conductivity, k

$$\Delta k = \pm 0.025 \text{ W/mK}$$

$$k = 0.41 \text{ W/mK}$$

$$A = 0.0005067 \text{ m}^2$$

$$L = 0.001905 \text{ m}$$

$$\Delta L = 0.0000508 \text{ m}$$

Uncertainty in \dot{Q}

$$\dot{Q} = \frac{kA}{L}(T_1 - T_2)$$

$$\frac{d\dot{Q}}{dk} = \frac{A}{L}(T_1 - T_2) \cdot \Delta k = \frac{0.0005067}{0.001905}(91.85 - 11.17) \cdot 0.025 = 0.5365$$

$$\frac{d\dot{Q}}{dA} = \frac{k}{L}(T_1 - T_2) \cdot \Delta A = \frac{0.41}{0.001905}(91.85 - 11.17) \cdot 0.000002027 = 0.0352$$

$$\frac{d\dot{Q}}{dL} = \frac{kA}{L^2}(T_2 - T_1) \cdot \Delta L = \frac{0.41(0.0005067)}{(0.001905)^2}(11.17 - 91.85) \cdot 0.0000508 = -0.2346$$

$$\frac{d\dot{Q}}{dT_1} = \frac{kA}{L} \cdot \Delta T_1 = \frac{0.41(0.0005067)}{0.001905} \cdot 0.5 = 0.0545$$

$$\frac{d\dot{Q}}{dT_2} = -\frac{kA}{L} \cdot \Delta T_2 = -\frac{0.41(0.0005067)}{0.001905} \cdot 0.5 = -0.0545$$

$$\omega_{\dot{Q}} = \sqrt{\left(\frac{d\dot{Q}}{dk} \cdot \Delta k\right)^2 + \left(\frac{d\dot{Q}}{dA} \cdot \Delta A\right)^2 + \left(\frac{d\dot{Q}}{dL} \cdot \Delta L\right)^2 + \left(\frac{d\dot{Q}}{dT_1} \cdot \Delta T_1\right)^2 + \left(\frac{d\dot{Q}}{dT_2} \cdot \Delta T_2\right)^2} =$$

$$\sqrt{(0.5365)^2 + (0.0352)^2 + (-0.2346)^2 + (0.0545)^2 + (-0.0545)^2}$$

$$= 0.592 \text{ W}$$

Uncertainty in the heat transfer coefficient, h

$$h = \frac{\dot{Q}/A}{T_1 - T_2}$$

$$\frac{dh}{dQ} = \frac{1}{A(T_1 - T_2)} \cdot \Delta Q = \frac{1}{0.0005067(91.85 - 11.17)} \cdot 0.592 = 14.481$$

$$\frac{dh}{dA} = -\frac{\dot{Q}}{A^2(T_1 - T_2)} \cdot \Delta A = -\frac{8.87}{0.0005067^2(91.85 - 11.17)} \cdot 0.000002027 = -0.868$$

$$\frac{dh}{dT_1} = -\frac{\dot{Q}}{A(T_1 - T_2)^2} \cdot \Delta T_1 = -\frac{8.87}{0.0005067(91.85 - 11.17)^2} \cdot 0.5 = -1.345$$

$$\frac{dh}{dT_2} = \frac{\dot{Q}}{A(T_1 - T_2)^2} \cdot \Delta T_2 = \frac{8.87}{0.0005067(91.85 - 11.17)^2} \cdot 0.5 = 1.345$$

$$\omega_h = \sqrt{\left(\frac{dh}{dQ} \cdot \Delta Q\right)^2 + \left(\frac{dh}{dA} \cdot \Delta A\right)^2 + \left(\frac{dh}{dT_1} \cdot \Delta T_1\right)^2 + \left(\frac{dh}{dT_2} \cdot \Delta T_2\right)^2} =$$

$$= \sqrt{(14.481)^2 + (-0.868)^2 + (-1.345)^2 + (1.345)^2} = \mathbf{14.63 \text{ W/m}^2\text{K}}$$

Therefore,

$$\mathbf{h = 216.89 \pm 14.63 \text{ W/m}^2\text{K}}$$

$$\mathbf{\%Error = \frac{14.63}{216.89} \cdot 100\% = 6.75\%}$$

Uncertainty Analysis (5 Mesh Stainless Steel @200°F and 399.89 PSI)

Uncertainty in Temperature Measurement from K-Type Thermocouples
 $\Delta T_1 = \pm 0.5^\circ\text{C}$

$$\Delta T_2 = \pm 0.5^\circ\text{C}$$

Uncertainty in Area

$$A = \frac{\pi}{4} D^2 \qquad \frac{dA}{dD} = \frac{\pi}{2} D \cdot \Delta D$$

Values

$$\Delta D = 2 \text{ mil} = .002 \text{ inch} = 0.0000508 \text{ m}$$

$$D = 1 \text{ inch} = 0.0254 \text{ m}$$

$$\omega_A = \sqrt{\left(\frac{dA}{dD} \cdot \Delta D\right)^2} = \sqrt{\left(\frac{\pi}{2}(0.0254)(0.0000508)\right)^2} = 0.000002027 \text{ m}^2$$

Uncertainty in thermal conductivity, k

$$\Delta k = \pm 0.028 \text{ W/mK}$$

$$k = 0.47 \text{ W/mK}$$

$$A = 0.0005067 \text{ m}^2$$

$$L = 0.001905 \text{ m}$$

$$\Delta L = 0.0000508 \text{ m}$$

Uncertainty in \dot{Q}

$$\dot{Q} = \frac{kA}{L}(T_1 - T_2)$$

$$\frac{d\dot{Q}}{dk} = \frac{A}{L}(T_1 - T_2) \cdot \Delta k = \frac{0.0005067}{0.001905}(91.89 - 13.15) \cdot 0.028 = 0.701$$

$$\frac{d\dot{Q}}{dA} = \frac{k}{L}(T_1 - T_2) \cdot \Delta A = \frac{0.47}{0.001905}(91.89 - 13.15) \cdot 0.000002027 = 0.0394$$

$$\frac{d\dot{Q}}{dL} = \frac{kA}{L^2}(T_2 - T_1) \cdot \Delta L = \frac{0.47(0.0005067)}{(0.001905)^2}(13.15 - 91.89) \cdot 0.0000508 = -0.2625$$

$$\frac{d\dot{Q}}{dT_1} = \frac{kA}{L} \cdot \Delta T_1 = \frac{0.47(0.0005067)}{0.001905} \cdot 0.5 = 0.0625$$

$$\frac{d\dot{Q}}{dT_2} = -\frac{kA}{L} \cdot \Delta T_2 = -\frac{0.41(0.0005067)}{0.001905} \cdot 0.5 = -0.0625$$

$$\omega_{\dot{Q}} = \sqrt{\left(\frac{d\dot{Q}}{dk} \cdot \Delta k\right)^2 + \left(\frac{d\dot{Q}}{dA} \cdot \Delta A\right)^2 + \left(\frac{d\dot{Q}}{dL} \cdot \Delta L\right)^2 + \left(\frac{d\dot{Q}}{dT_1} \cdot \Delta T_1\right)^2 + \left(\frac{d\dot{Q}}{dT_2} \cdot \Delta T_2\right)^2} =$$

$$\sqrt{(0.701)^2 + (0.0394)^2 + (-0.2625)^2 + (0.0625)^2 + (-0.0625)^2}$$

$$= 0.755 \text{ W}$$

Uncertainty in the heat transfer coefficient, h

$$h = \frac{\dot{Q}/A}{T_1 - T_2}$$

$$\frac{dh}{dQ} = \frac{1}{A(T_1 - T_2)} \cdot \Delta Q = \frac{1}{0.0005067(91.89 - 13.15)} \cdot 0.755 = 18.923$$

$$\frac{dh}{dA} = -\frac{\dot{Q}}{A^2(T_1 - T_2)} \cdot \Delta A = -\frac{9.81}{0.0005067^2(91.89 - 13.15)} \cdot 0.000002027 = -0.9836$$

$$\frac{dh}{dT_1} = -\frac{\dot{Q}}{A(T_1 - T_2)^2} \cdot \Delta T_1 = -\frac{9.81}{0.0005067(91.89 - 13.15)^2} \cdot 0.5 = -1.561$$

$$\frac{dh}{dT_2} = \frac{\dot{Q}}{A(T_1 - T_2)^2} \cdot \Delta T_2 = \frac{9.81}{0.0005067(91.89 - 13.15)^2} \cdot 0.5 = 1.561$$

$$\omega_h = \sqrt{\left(\frac{dh}{d\dot{Q}} \cdot \Delta \dot{Q}\right)^2 + \left(\frac{dh}{dA} \cdot \Delta A\right)^2 + \left(\frac{dh}{dT_1} \cdot \Delta T_1\right)^2 + \left(\frac{dh}{dT_2} \cdot \Delta T_2\right)^2} =$$

$$= \sqrt{(18.923)^2 + (-0.9836)^2 + (-1.561)^2 + (1.561)^2} = \mathbf{19.08 \text{ W/m}^2\text{K}}$$

Therefore,

$$\mathbf{h = 245.83 \pm 19.08 \text{ W/m}^2\text{K}}$$

$$\mathbf{\%Error = \frac{19.08}{245.83} \cdot 100\% = 7.76\%}$$

APPENDIX C- WIRE SCREEN LITERATURE

For future consideration in Phase II and III – Pipe Prototype Construction

CHOICE OF MESH GEOMETRY

Largest Open Area

- Architectural Type
- Veil, Strand
- Flexible
- Plain Weave
- Open Area: 76%
- Weld Points: medium
- Weight: 0.75 lbs/sq-ft
- Circular Cross Section Wire



Courtesy of Architecturalmesh.com

Lowest Weight

- Architectural Type
- Drape, Corduroy
- Flexible
- Plain Weave
- Open Area: 74%
- Weld Points: medium
- Weight: 0.55 lbs/sq-ft
- Circular Cross Section Wire



Non-Circular Wire Cross Section

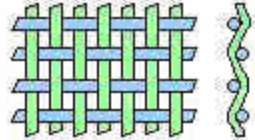
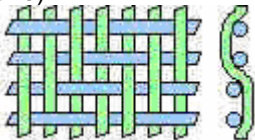
- Architectural Type
- Veil, Cubist
- Flexible
- Not Plain Weave
- Open Area: 74%
- Weld Points: questionable
- Weight: 2.2lbs/sq-ft
- Non-Circular Cross Section Wire

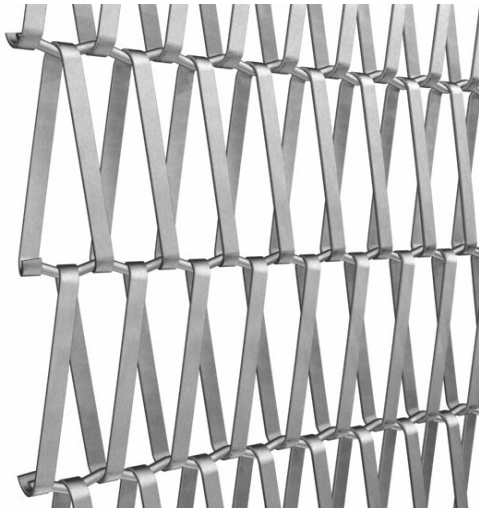


Most Choices for Weld Points

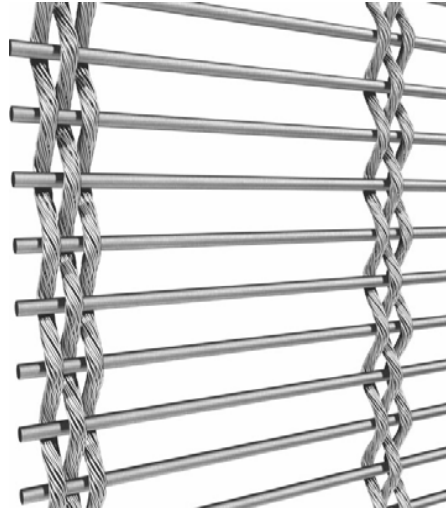
- Architectural Type
- Drape, Rib Knit
- Flexible
- Plain Weave
- Open Area: 75%
- Weld Points: many
- Weight: 0.783 lbs/sq-ft
- Oval Cross Sectional Area



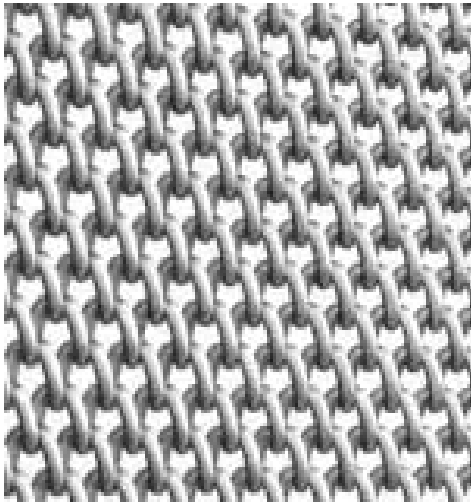
Drape	Type of architectural wire mesh.
Flexible	The ability to behave in a ductile manner.
Hydrostatic Pressure Fitting	Wire mesh is spot welded to the interior of the outer pipe, the inner pipe is placed inside the outer pipe then the controlled application of pressure allows the inner pipe to expand (Kidwell, 3).
Plain Weave	Wires of mesh over lap each other (one over one).  (Lenntech.com)
Shrink Fitting	Wire mesh is spot welded to the inner pipe and then cooled, the outer pipe is heated and placed over the inner pipe (and mesh) then allowed to cool and shrink over the inner pipe (Kidwell, 3).
Twill Weave	Wires of mesh over lap each other (one over two).  (Lenntech.com)
Veil	Type of architectural wire mesh
Weld Points	Contact points between wire mesh and pipe.



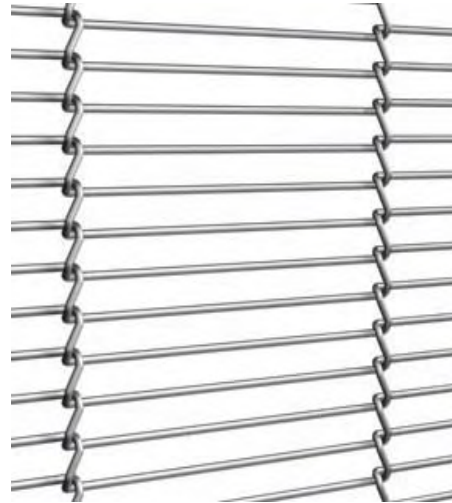
Balance



Braid



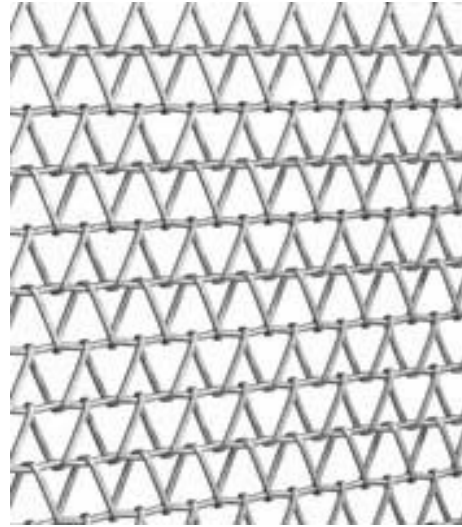
Chain



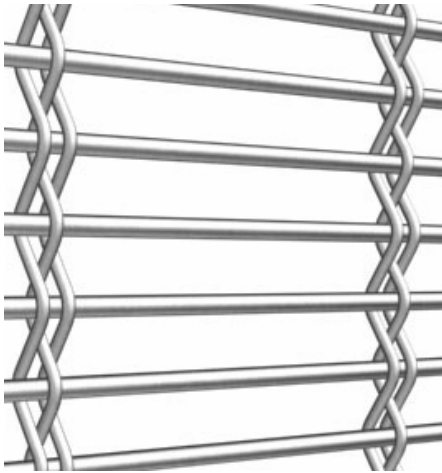
Corduroy



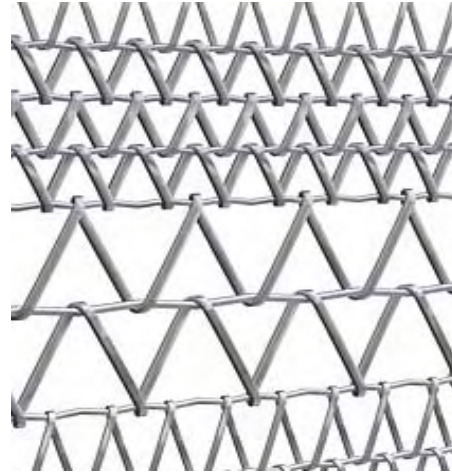
Cubist



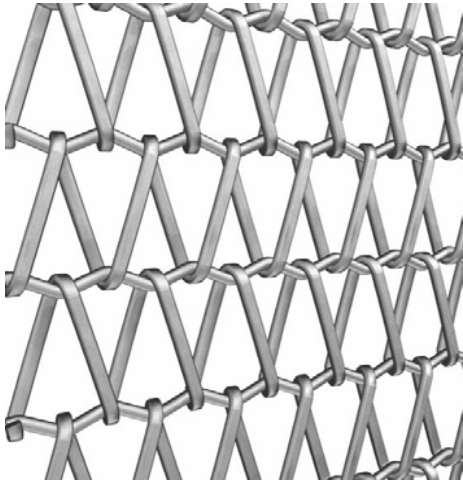
Microbalance



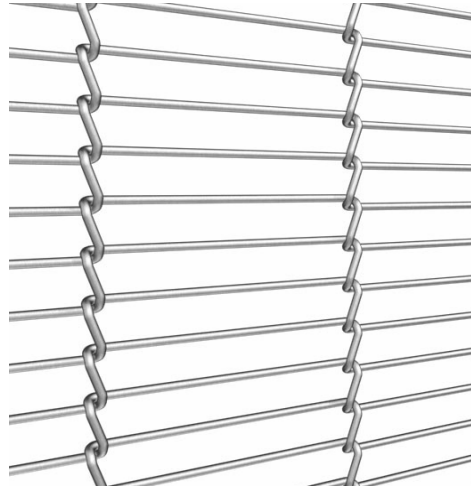
Plait



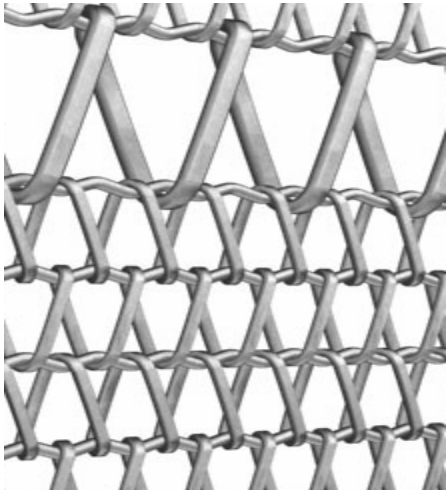
Rib Knit



Scale



Strand



Stripe

Conversion Factors for Different Units of Measurements			
Quantity	SI Unit	Other Unit	Inverse Factor
Length	1 m	3.281 feet (ft)	0.3048 m
	1 km	0.540 nautical miles	1.852 km
	1 km	0.6213712 mile	1.609344 km
Area	1 m ²	10.764 ft ²	0.0929m ²
Volume	1 m ³	35.315 ft ³	0.0283 m ³
	1 m ³	264.2 gallon (US)	0.00379 m ³
	1 m ³	220.0 gallon (UK)	0.00455 m ³
	1 m ³	6.29 barrel (US Petroleum)	0.1589 m ³
Velocity	1 m/s	3.281 ft/s	0.305 m/s
	1 m/s	1.943 knot	0.515 m/s
	1 m/s	2.2369 mph	0.44704 m/s
	1 km/hr	0.62137 mph	1.6093 km/hr
Mass	1 kg	2.205 pound	0.454 kg
	1 Mg	0.984 ton (long)	1.016 Mg
	1 Mg	1 tonne (metric)	1 Mg
Force	1 N	0.225 pound force	4.448 N
	1 MN	100.4 ton force	9964 N
	1 MN	224.81 kip	4448 N
Pressure	1 N/m ²	0.000145 psi	6895 N/m ²
	1 MN/m ²	20.885 kip/ft ²	47880 N/m ²
Energy	1 J	0.738 foot pounds	1.356 J
Power	1 W	0.00134 horsepower	745.7 W
Temperature	0 ^o Celsius	32 ^o Fahrenheit	-17.78 ^o Celsius
Frequency	1 cycle/s	1 hertz	1 cycle/second
Flow Rates	1 m ³ /day	6.289 barrel/day	0.1589 m ³ /day
	1 m ³ /day	35.3146 ft ³ /day	0.0283 m ³ /day
Density	1 g/cm ³	0.578 oz./inch ³	1.73 g/cm ³